Atmospheric Pollution Research 17 (2026) 102861

Contents lists available at ScienceDirect

Atmospheric Pollution Research

journal homepage: www.elsevier.com/locate/apr

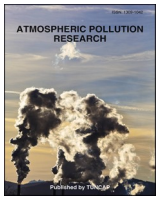

Heating transformation in winter significantly will reduce GHGs (CO_2, CH_4, N_2O) emissions: implication from multiple-year concentration observations in Beijing

Wenjing Huang [a], Wei Xiao [b,*], Xuefa Wen [c], Jie Wei [c], Sidan Lyu [c], Cheng Hu [d], Mi Zhang [b], Ning Hu [b], Xuhui Lee [e]

[a] Jiangsu Key Laboratory of Atmospheric Environment Monitoring and Pollution Control, Collaborative Innovation Center of Atmospheric Environment and Equipment Technology, School of Environmental Science and Engineering, Nanjing University of Information Science and Technology, Nanjing, 210044, China
[b] International Joint Laboratory on Climate and Environment Change, Nanjing University of Information Science and Technology, Nanjing, 210044, China
[c] Key Laboratory of Ecosystem Network Observation and Modeling, Institute of Geographic Sciences and Natural Resources Research, Chinese Academy of Sciences, Beijing, 100101, China
[d] Co-Innovation Center for Sustainable Forest in Southern China, Nanjing Forestry University, Nanjing, 210037, China
[e] School of Forestry and Environmental Studies, Yale University, New Haven, 06511, CT, USA

ARTICLE INFO

Keywords:
Energy structure
CH_4/CO_2 ratio
N_2O/CO_2 ratio
GHG emissions
Beijing

ABSTRACT

It is widely acknowledged that government policies significantly influence the emission and distribution of urban greenhouse gases (GHGs). However, accurately assessing the impact of urban pollution control measures on GHGs in megacities remains challenging and relies on integrating model simulations with multi-source observational data. Since 2003, Beijing, the capital of China, has gradually expanded a heating transformation policy from the city center. This policy shift offers a unique opportunity to quantify the reduction in urban GHG emissions resulting from government interventions. Based on urban GHG observations in Beijing from 2015 to 2020 (conducted without a drying system), this study applies an atmospheric method to analyze interannual variations in GHG emissions during winter heating seasons, which coincided with the energy structure transition, and identifies the main drivers of the observed trends in CH_4/CO_2 and N_2O/CO_2 ratios. Our findings showed that: (1) the shift in energy structure has directly reduced greenhouse gas emissions, thereby significantly impacting Beijing's seasonal GHG concentration trends, with an average annual winter reduction of 5.30×10^5 t of CO_2-equivalent between 2015 and 2018.; (2) the CH_4/CO_2 and N_2O/CO_2 ratios exhibited distinct winter trends during 2015–2020, ranging between $6.02 \times 10^{-3} - 8.39 \times 10^{-3}$ ppm ppm^{-1} and $5.60 \times 10^{-5} - 8.88 \times 10^{-5}$ ppm ppm^{-1}, respectively; (3) source diagnostics derived from the inter-gas correlations show that the interannual variations were driven by both the coal-to-gas transition and other anthropogenic sources like coal mining, wastewater treatment, and landfill management. This study focuses on Beijing, a city that has undergone significant energy structure changes, and serves as a case study for other cities undergoing similar transformations. While this practice can reduce GHG emission intensity, the increased use of natural gas may introduce other emission challenges that require further investigation.

1. Introduction

Cities are major contributors to greenhouse gas (GHG) emissions, with more than 70 % of CO_2 emissions arising from fossil fuel combustion. The concentrated use of fossil fuels, combined with urbanization-driven land-use changes, makes cities hotspots for CO_2 and CH_4 emissions (Hutyra et al., 2014; Mitchell et al., 2018). While CO_2 persists in the atmosphere for 50–200 years (Lelieveld et al., 1998), CH_4, with its 100-year global warming potential (GWP-100) 28 times that of CO_2 and a relatively short atmospheric lifetime of 9–10 years (Dlugokencky et al., 2011; IPCC, 2021), presents a critical near-term mitigation opportunity (Archer and Brovkin, 2008; Nisbet et al.,

* Corresponding author.
E-mail addresses: 1546112531@qq.com (W. Huang), wei.xiao@nuist.edu.cn (W. Xiao), wenxf@igsnrr.ac.cn (X. Wen), weijie@igsnrr.ac.cn (J. Wei), lvsidan@igsnrr.ac.cn (S. Lyu), nihaohucheng@163.com (C. Hu), zhangm.80@nuist.edu.cn (M. Zhang), huning@nuist.edu.cn (N. Hu), Xuhui.lee@yale.edu (X. Lee).

https://doi.org/10.1016/j.apr.2025.102861
Received 2 June 2025; Received in revised form 9 December 2025; Accepted 11 December 2025
Available online 12 December 2025

2020). Global CH_4 emissions from fossil fuel production and use account for 17 % (bottom-up) or 19 % (top-down) between 2008 and 2017, a share which increases to 45 % (bottom-up) or 57 % (top-down) when including emissions from wastewater treatment, landfilling, and agriculture (Saunois et al., 2020). N_2O is a long-lived gas with a GWP-100 273 times that of CO_2 and an atmospheric lifetime of 116 ± 9 years (Prather et al., 2015). Its anthropogenic emissions, primarily from agricultural practices like fertilizer use and animal waste management (Galloway et al., 2008), are notoriously difficult to quantify and control (Prather et al., 2009; Ciais et al., 2014). Long-term, high-precision, multi-species GHG observations in urban areas provide the essential data required not only for developing process-based models but also for formulating evidence-based mitigation strategies that account for the contributions of individual gases (Allen et al., 2022; Meurer et al., 2016; Turner et al., 2019). This approach is vital for reducing uncertainties in temperature projections and for quantifying non-climate co-benefits, particularly in the case of CH_4 (Shindell et al., 2017).

Understanding the impact of policy implementation in urban settings provides valuable insights for predicting China's future development paths. In Beijing, a city undergoing significant energy transitions, traffic emissions are the primary source of CO_2 (75.5 % in summer and 38.9 % in winter), whereas in winter, heating contributes a nearly equal proportion of 38.3 % (Song et al., 2013). Between 2007 and 2015, Beijing's energy transformation entered its fourth phase (Zhang et al., 2018). During the Thirteenth Five-Year Plan (2016–2020), Beijing's energy structure was adjusted, with coal use in the heating sector decreasing from 31.1 % in 2010–2011 to 0 % in 2018–2019. At the same time, gas and electricity use increased from 44.1 % to 69.2 % and from 1.7 % to 6.4 %, respectively (Zhou, 2020). However, there are unresolved issues in the quantified emission assessments of Beijing's energy transition. Remarkably, the outbreak of the Coronavirus Disease 2019 (COVID-19) in late December 2019 provided an unintended yet valuable opportunity to assess the impacts of shifts in energy structure and reduced consumption on GHG and pollutant emissions, as well as on extreme weather events (Liu et al., 2021; Yang et al., 2022; Zhang et al., 2021).

The impact of urbanization on GHG emissions, particularly CH_4 and N_2O, has not been comprehensively quantified, especially at the city scale. Top-down approaches have demonstrated useful as independent assessments of GHG emission inventories at national and regional levels (Chen and Prinn, 2006; Dai et al., 2016; Hu et al., 2019). However, studies that encompass all three major anthropogenic GHGs—CO_2, CH_4, and N_2O—are rare. In 2007, CH_4 and N_2O in China's 26 industrial sectors accounted for 14.3 % of total GHG emissions, when converted to CO_2 equivalents, and this proportion has steadily increased (Chen and Zhang, 2010; EPA, 2012). Climate change mitigation policies can effectively reduce costs in three dimensions: spatial, temporal, and by gas species (Kurosawa, 2006). China's 2020 carbon peak and neutrality targets emphasize the need for accurate quantification of multiple gases at the urban scale, crucial for assessing and optimizing policy options tailored to specific conditions.

Quantifying urban emissions is challenging due to the considerable temporal and spatial variability of emission sources. Traffic patterns, along with weather-induced heating and cooling, are key factors influencing these emissions. Current direct observations and modeling efforts in urban areas primarily focus on CO_2 emissions (Baldocchi et al., 2001; Mallia et al., 2020; Wang et al., 2020). In contrast, CH_4 and N_2O emissions in urban settings are typically estimated using bottom-up methods, which are limited by the availability of data at such sites. Zazzeri et al. (2017) leverages mobile sampling and $\delta^{13}C$-CH_4 isotopic measurements, demonstrating that urban CH_4 emissions are dominated by fossil fuel sources (e.g., gas leaks), contrary to inventories which often overestimate waste-related emissions. Notably, the correlation between CH_4 and CO_2 emissions differs between Miyun and Dashiwo, suggesting that the two gases share a common emission source within the same area of influence and under similar atmospheric transport conditions. A closer correlation between these two gases indicates more consistent source contributions. Through combined analysis of gas correlations and back trajectory analysis, the emissions regimes at Miyun and Dashiwo are distinguished as a single dominant combustion/respiration source versus multiple non-combustion methane sources, respectively (Munger et al., 2020). A tower-based study in Edinburgh, UK, employed the eddy-covariance method to measure N_2O emissions, which correlated well with emissions of the anthropogenic tracers CO and CO_2, demonstrating good agreement with the urban source and vehicle traffic emission ratios derived from the National Atmospheric Emissions Inventory (Famulari et al., 2010).

Achieving the 2060 carbon neutrality target requires a systematic nationwide transition towards "de-coalization". In Beijing, China's capital, a coal-free heating energy structure has been largely established, significantly improving air quality (Li et al., 2020). Given the alignment between carbon neutrality and air quality objectives, further quantification and source apportionment of GHG emissions in urban areas like Beijing are crucial, especially during this transitional period. This study conducted atmospheric concentration observations in Beijing from 2015 to 2020 with two objectives: (1) to estimate the interannual variation of GHG emissions associated with winter heating, and (2) to assess whether the energy structure transformation has effectively reduced emissions.

2. Methodology

2.1. Site and observations

Atmospheric concentrations of CO_2, CH_4, and N_2O were measured at the Institute of Geographic Sciences and Natural Resources Research, Chinese Academy of Sciences (IGSNRR-CAS). IGSNRR-CAS, located in northern Beijing (40°00′N, 116°23′E, 45 m above sea level; Fig. 1), offers a strategic location for environmental assessments. Beijing's land use is diverse, comprising forests (47.6 %), croplands (24.6 %), impervious surfaces (15.5 %), grasslands (7.8 %), shrublands (2.6 %), water bodies (1.5 %), barelands (0.3 %), and wetlands (0.1 %) (Gong et al., 2019; source: http://data.ess.tsinghua.edu.cn/). Major agricultural crops in Beijing include corn, vegetables, and winter wheat (Beijing Statistical Yearbook, 2020). Additionally, Beijing contributes 3.6 % of China's GDP while occupying only 0.2 % land area (China Statistical Yearbook, 2020). The heating season in Beijing, defined from December to February, is based on historical heating durations and is commonly referred to as the cold season. The other three seasons are classified as spring (March to May), summer (June to August), and autumn (September to November).

The atmospheric observations were conducted from March 21, 2015, to December 31, 2020. The air intake was located outdoors, approximately 10 m above ground level, next to the laboratory. Air was drawn through Teflon tubing into the analyzer (model G2508, Picarro Inc., Santa Clara, California, USA), passing sequentially through filters with pore sizes of 2 μm (Swagelok JP5627001) and 30 μm (Xiongchuan SS-224F). The 2 μm filter was positioned at the air intake, and the 30 μm filter was placed at the analyzer's entrance. An external rotary valve, installed between the filters, directed the gas flow through one of four pathways: the external atmosphere or one of three standard gas lines—each containing different concentrations of CO_2, CH_4, and N_2O. Reported CH_4, CO_2 and N_2O concentrations in this study are dry mole fractions, corrected in real-time for water vapor dilution by the analyzer (Text S1). The instrument measurement rate was approximately 0.2 Hz. The raw data were processed in half-hour blocks, with outliers identified as values exceeding 1.5 times the standard deviation from a five-point moving average and subsequently removed.

The analyzer performed a calibration cycle every 5 h, measuring three concentration levels (high, low, and median) over 15 min, with 5 min allocated to each level. Details of the standard gases are provided in Table S1. Transition periods between gases lasted approximately 16 s before signal stabilization, compared to the instrument's typical 10–90 % gas response time of ~8 s. These transition intervals were

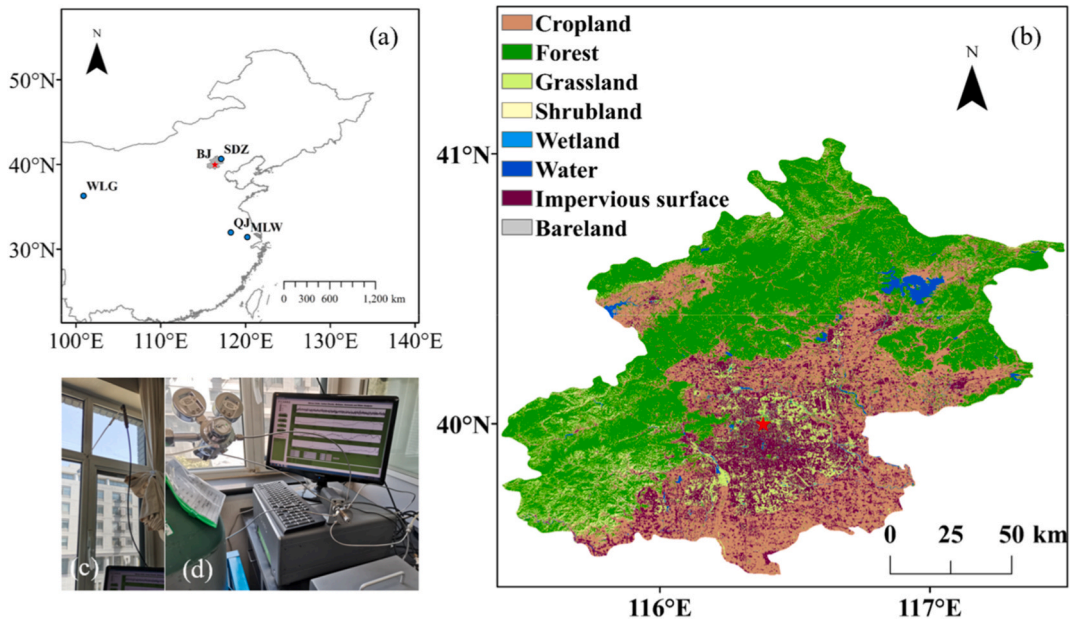

Fig. 1. Site location and instrumentation. (a) Geographical distribution of the observation site (highlighted) and four other reference sites. (b) Land cover map of Beijing at a 30-m spatial resolution (adapted from Gong et al., 2019). (c) Photograph showing the instrument air inlet at 10 m above ground level. (d) Photograph of the instrument.

systematically excluded during data processing. For the remaining stable data, a 3-min moving window was applied, and the window with the smallest standard deviation was selected to determine the mean value as the final instrument reading. A two-point calibration was applied for each gas using reference standards at varying concentration levels. Stable measurement intervals during standard injections were averaged and linearly regressed against reference values to derive calibration functions. Data between consecutive calibrations were corrected using the equation from the subsequent calibration event, and the final corrected value was determined as the average of the corrections applied from both adjacent calibration periods. Subsequently, validated data were aggregated into half-hourly mean concentrations for analysis.

Additionally, this study compared the concentration profiles of the urban site in Beijing with those from several representative non-heating winter sites. For a detailed description of the sites, see Table S2. The Meiliangwan (MLW) and Quanjiao (QJ) sites are located in Wuxi, Jiangsu Province, and Chuzhou, Anhui Province, respectively, where winter heating is absent. The Waliguan (WLG) site is a GAW Global station, part of the World Meteorological Organization's Global Atmosphere Watch Programme, located in China. The Shangdianzi GAW Regional Station (SDZ) is located 150 km northeast of urban Beijing.

2.2. Atmospheric method

Jaffe et al. (2005) used the slopes of A vs B correlations to determine emission ratios based on the following assumptions: (1) no loss of substances during transport; (2) constant sources with fixed emission ratios; and (3) constant background concentrations throughout the event. Assumption (2) can be extended to multiple sources along an event's trajectory, as long as their relative contributions remain constant throughout the event (Brunke et al., 2012).

$$\text{B metric tons} = (\text{A metric tons})(B_{atm} / A_{atm})(M_B / M_A) \quad (1)$$

The atmospheric method uses a well-understood and quantifiable gas (A) to trace another gas (B). This method combines the observed atmospheric concentration ratio (B_{atm}/A_{atm}) with emissions of A to estimate emissions of B. In this study, CO_2 was selected as the tracer gas to quantify CH_4 and N_2O emissions in Beijing, with CO_2 emissions obtained from inventory data. Given the uncertainties in the observed concentrations of CO_2, CH_4 and N_2O, geometric mean regression was chosen as the fitting method, which will be detailed in the following section.

Considering the assumptions inherent in the method, winter daytime (11:00–16:00; Fig. S1) was selected to constrain anthropogenic CH_4 and N_2O emissions in Beijing. The planetary boundary layer height, simulated by WRF, exceeds 300 m during this period, indicating that the atmosphere is well mixed and there is no significant disturbance from nearby direct emissions. However, winter heating in Beijing introduces additional anthropogenic emissions compared to other seasons. Therefore, distinguishing heating emissions from other anthropogenic sources is a challenge this study seeks to address.

2.2.1. Footprint analysis

In this study, January 2016 was selected as a representative month of the cold season to analyze the source contribution area for the winter observation point concentration. The WRF-STILT model was employed to quantify the source area contributing to the observed concentration at the site. The spatial distribution of the source contribution footprint was determined using the Weather Research and Forecasting (WRF) model (version 3.8.1) in conjunction with the Stochastic Time-Inverted Lagrangian Transport (STILT) model. This combined approach used three nested domains with spatial resolutions of 9, 3, and 1 km (Fig. 2; Lin et al., 2003; Skamarock and Klemp, 2008). Beijing was located in Domain 3 (d03), which had the highest spatial resolution, while Domain 2 (d02) covered the Beijing-Tianjin-Hebei region. This configuration helped understand the influence of external areas on the observation point. The WRF model provided hourly gridded meteorological data for the region of interest, based on reanalysis data. The STILT model then used these meteorological data to backtrack air particles in time, assessing their sensitivity to surface fluxes of specific gases. Further details can be found in Lin et al. (2003); Gerbig et al., 2003. These particles were employed to calculate a footprint with a spatial resolution of $0.1^\circ \times 0.1^\circ$ [unit: ppm (μmol m^{-2} s^{-1})$^{-1}$], delineating the upstream area that influences the air arriving at a specific location (Gerbig et al., 2003a, 2003b).

2.2.2. Inventory products

Inventory products can be divided into two categories: (1) those

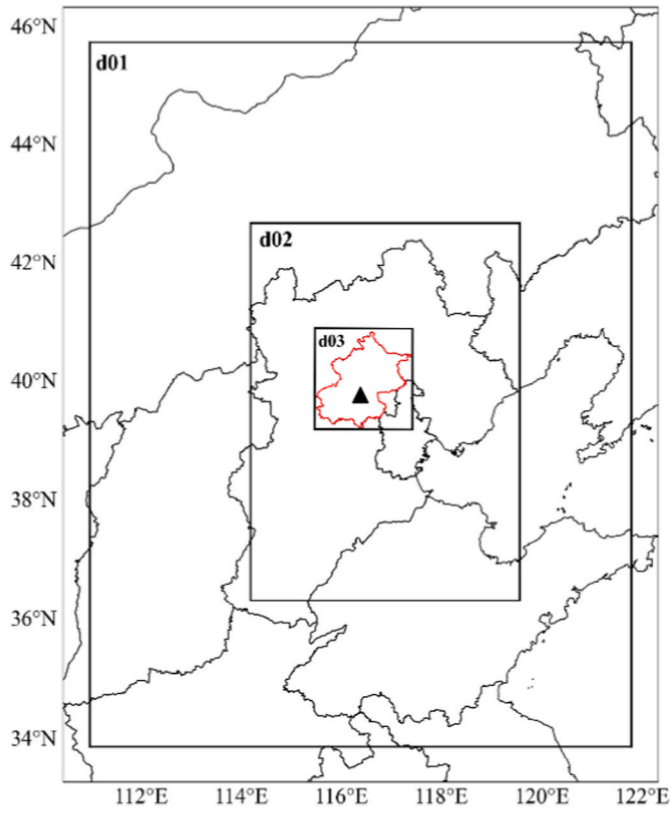

Fig. 2. Three domains configuration used in WRF. The spatial resolutions for d01, d02, and d03 are 9 km, 3 km, and 1 km, respectively. The red line delineates the boundary of Beijing municipality. The triangles indicate the locations of the observation sites.

based on provincial or national-level statistical data, such as the Open-source Data Inventory for Anthropogenic CO_2, version 2019 (ODIAC, 2019), the Emissions Database for Global Atmospheric Research, version 60 (EDGAR v6.0), and the Fossil Fuel Data Assimilation System, version 2.2 (FFDAS v2.2) (Table 1); and (2) those based on city-level statistical data, including the Multi-resolution Emission Inventory for China (MEIC v1.3), China Emission Accounts and Datasets (CEADs), and the Global infrastructure Emission Database (GID). These datasets can be spatially allocated using proxies, such as nighttime light intensity or population density. To achieve a realistic spatial distribution of emissions from specific industrial sources, such as cement and power plants, emissions are modeled using point source data, while traffic emissions are based on line source data. The spatial resolution of these inventory products ranges from 1 km (ODIAC and FFDAS) to 0.25° (approximately 27.5 km). For more details on these inventory products, refer to Han et al. (2020a, 2020b).

Given the limitations in directly comparing current emission statistics with top-down results at the city scale, it is crucial to filter and eliminate redundant emission sources across various emission inventories (Chen et al., 2020). Within city boundaries, only direct emissions from fossil fuel combustion, industrial production and processes, transportation, land use, and waste (scope 1) should be considered for comparison with observational inversion results. Emissions from total electricity consumption generated both within and outside city boundaries, as well as emissions from aviation and marine sources, and upstream power plant emissions, should be excluded from this analysis.

Table 1
Summary of the CO_2 emission inventories (modified from Han et al., 2020). The products marked with an asterisk (*) have no relevant data in this study.

Data description	ODIAC	EDGAR	PKU-CO_2*	FFDAS	CHRED*	MEIC	NJU*	CEADs	GID
Domain	Global	Global	Global	Global	China	China	China	China	China
Temporal resolution	Monthly	Monthly	Monthly	Hourly/Annual	Biennially or triennially	Monthly	Annual	Annual	Annual
Spatial resolution	1 km	0.1°	0.1°	0.1°/1 km	10 km	0.25°	0.25°	N/A	0.1°
Emission estimates	Global/National	Global/National	Global/National	Global/National	National/Provincial	National/Provincial	National/Provincial	Prefectural/National/Provincial	National/Provincial
National uncertainty	17.5 % (95 % CI)	±15 %	±19 % (95 % CI)	5–15 %	±8 %	±15 %	7–10 % (90 % CI)	15 % – 25 % (95 % CI)	N/A
Point source	CARMA2.0	CARMA3.0	CARMA2.0	CARMA2.0	FCPSC	CPED	CEC; ACC; CCTEN	N/A	FCPSC; GPED
Line source	N/A	The Open-StreetMap and Open-RailwayMap, Int. aviation and bunker	N/A	Transport networks	The national road, railway, navigation, and traffic flows	Transport networks	N/A	N/A	N/A
Area source	Nighttime light	Population density, Nighttime light	Vegetation population density, nighttime light	Nighttime light	Population density, land use, human activity	Population density, land use	Population density, GDP	N/A	N/A
Latest year	2018	2018	2014	2015	2012	2017	2017	2017	2019
References	Oda et al. (2018)	Janssens-Maenhout et al. (2019)	Wang et al. (2013)	Asefi-Najafabady et al. (2014)	Cai et al. (2018) Wang et al. (2014)	Liu et al. (2015) Zheng et al. (2018)	Liu et al. (2013)	Guan et al. (2018) Shan et al. (2018)	Tong et al. (2019)

3. Results

3.1. Temporal variations of CO_2, CH_4 and N_2O concentration

The multi-year atmospheric concentrations of CO_2, CH_4, and N_2O at various sites are presented in Fig. 3. Due to the limited availability of high-precision, long-term concentration measurements, the comparative data from other referenced sites are available only for partial periods. Each data point in the figure represents the monthly average concentration, with detailed half-hourly observational data provided in Fig. S2. Significant data gaps from December 2019 to March 2020 were caused by the suspension of instrument maintenance during the COVID-19 lockdown. Notably, six-year continuous concentration observations show that 2017 marked a turning point, after which the sharp increase in CO_2 and CH_4 concentrations during the cold season subsided. During the annual cold season, the CO_2 concentration at our site continues to rise, in contrast to regions like the Yangtze River Delta, which lack central heating. The CO_2 concentration at the SDZ site is between those observed in Beijing (BJ) and WLG. Although SDZ is located in the rural outskirts of Beijing, the wintertime monthly average CO_2 concentration difference between SDZ and BJ is 42.97 ppm, significantly higher than in summer (8.58 ppm). In contrast, in non-heating areas like QJ and MLW, the CH_4 concentration peaks in summer, while in Beijing, it peaks in November or December. Although all observation sites experience temperature and precipitation peaks in July and August, no distinct seasonal pattern for N_2O is observed in our data. However, similar to WLG, a clear year-on-year increase in N_2O concentration is observed.

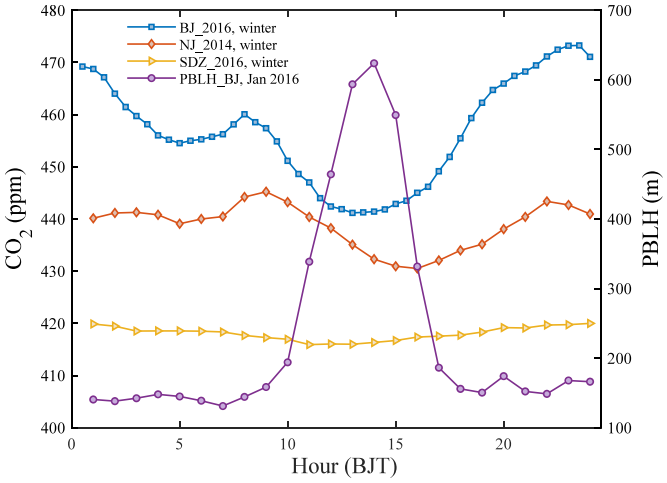

Fig. 4. Diurnal variation of CO_2 concentration in Beijing (BJ, Jan, Feb and Dec in 2016), Nanjing (NJ, Jan, Feb and Dec in 2014; Xu et al., 2017), and Shangdianzi (SDZ, Jan, Feb and Dec in 2016) and planetary boundary layer height (PBLH, Jan 2016) simulated by WRF. Figure axes display time in local time (Beijing Time, BJT=UTC+08:00). All subsequent time references in this study are based on Beijing Time unless otherwise specified.

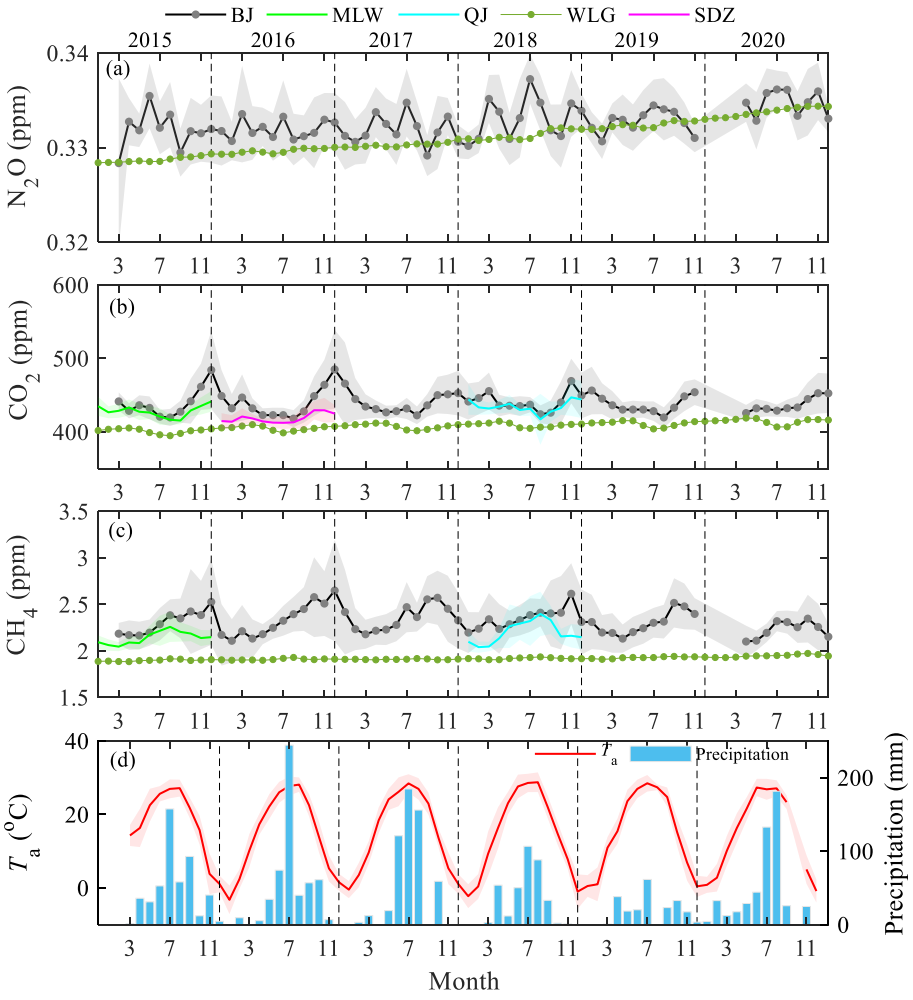

Fig. 3. Seasonal variation of (a) N_2O, (b) CO_2, (c) CH_4 concentration and (d) temperature and precipitation in Beijing and other comparison sites, including MLW, QJ, WLG and SDZ. The shaded areas represent the standard deviation intervals around the average.

Fig. 4 shows the diurnal variation in concentrations during the cold season, revealing distinct patterns for CO_2 in Beijing (with heating) and Nanjing (without heating), which differ from those at the regional background station SDZ. In Beijing, the daily maximum CO_2 concentration occurred at night (23:30), with a secondary peak before or after sunrise (8:00). The nadir, or lowest point, in concentration closely coincided with the peak in boundary layer height (13:00). In contrast, in Nanjing, the maximum CO_2 value was observed before or after sunrise (9:00), with a secondary peak at night (22:00), and the nadir occurred at 16:00.

3.2. Source contribution area

Further analysis is required to quantify the source regions contributing to our observations and assess their representativeness in reflecting changes in source and sink contributions in Beijing. Fig. 5 illustrates the footprint, or influence-weighting functions, of the area surrounding the observation site. The darker the color in Fig. 5, the greater the potential contribution to the observation site. Sensitive source areas were predominantly located in Beijing and the northwestern part of Hebei Province (Fig. 5b). Observations influenced by emissions from Hebei Province can be excluded from further analysis by considering wind direction (northwest winds), ensuring that the selected data primarily represent emissions within Beijing.

In this study, we employed a threshold of log10(footprint) greater than −3 to identify the most sensitive contributing area, distinct from the approaches of Chen et al. (2016) and Hu et al. (2018b), who utilized a threshold of 10^{-4} ppm (μmol m^{-2} s^{-1})$^{-1}$. Hu et al. (2018a) found that areas defined by a threshold of 10^{-3} ppm (μmol m^{-2} s^{-1})$^{-1}$ accounted for 80 % of CO_2 enhancement, compared to 90 % with a threshold of 10^{-4} ppm (μmol m^{-2} s^{-1})$^{-1}$. It is important to note that the footprint indicates only the potential contribution to the observation site; the enhancement also depends on emissions at grid points. Based on the spatial distribution of CO_2 emissions from the MEIC inventory and CH_4 and N_2O emissions from the EDGAR inventories, grid sites in Beijing exhibit higher CO_2 and N_2O emissions than those in surrounding areas. For CH_4, Beijing and its southern regions are emission hotspots. Focusing on CO_2 for quantitative analysis, we hypothesize that the emission grid within the simulated domain contributes fully to the observed concentration enhancement. Emissions between provinces are adjusted based on weight coefficients, with emissions within provinces assumed to be evenly distributed. These coefficients are derived from the emission ratio per unit area of contributing provinces in January 2016, with Beijing as the reference point. Consequently, it is estimated that the strong source area contributes 88 % to the concentration enhancement, with Beijing contributing 69 %. Although this scenario is based on an idealized hypothesis, it helps validate that grids with a footprint greater than 10^{-3} ppm (μmol m^{-2} s^{-1})$^{-1}$ are representative, and that observations made at a height of 10 m are significantly influenced by sources and sinks within the Beijing area.

3.3. The CH_4 and the N_2O versus CO_2 regression slopes

Figs. 6 and 7 show the regression results based on winter daytime observations from 2015 to 2018. Due to the lack of data from December 2019 to February 2020, the analysis was limited to winter data from 2015 to 2018. The data analyzed were the average daytime concentrations, after selecting for wind direction (0–270°). The slopes of the CH_4 versus CO_2 regression lines ranged from 5.60×10^{-5} to 8.88×10^{-5} ppm ppm^{-1}, with the highest slope in winter 2018 and the lowest in winter 2015.

The temporal trends in CH_4 and CO_2 concentrations were strongly correlated. The correlation coefficients (R) for the average daily concentrations from winters 2015 to 2018 exceeded 0.90. The slope of the linear fit between the two gases peaked at 0.0084 in winter 2016 and reached its lowest point at 0.0060 in winter 2017.

Additionally, we analyzed the regression slopes for CH_4 and N_2O versus CO_2 on a half-hourly basis, considering wind direction and speed (2 m s^{-1}) (Figs. S3 and S4). Data from northwest wind directions were excluded, as these conditions were associated with higher wind speeds and lower CO_2, CH_4, and N_2O concentrations. The slope values for these concentrations, especially the N_2O/CO_2 ratio, differed significantly from those observed under other wind directions, highlighting the importance of wind direction filtering. Table 2 summarizes the slope values across various conditions. The analysis revealed that the linear correlation between CH_4 and CO_2, as well as between N_2O and CO_2, is stronger on a daily scale than on a half-hourly scale, with the latter exhibiting larger slope values. This trend of increasing slope values was also observed after applying wind filtering, for both daily and half-hourly scales.

3.4. CO_2, CH_4 and N_2O emissions in Beijing

When comparing emission inventories for Beijing from various

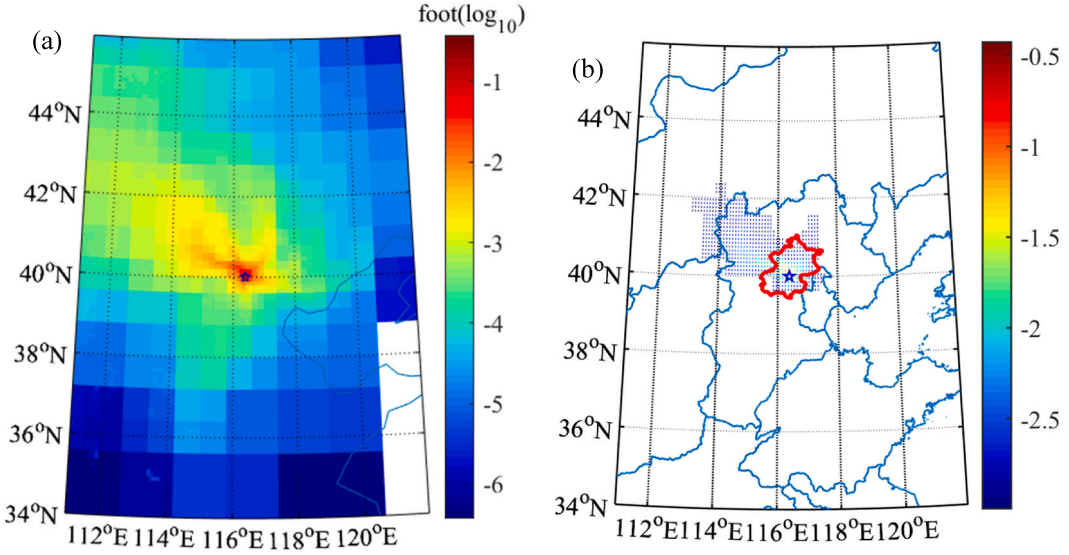

Fig. 5. (a) Average source footprints and (b) strong source area in Jan 2016 (units: $\log_{10}$(ppm (μmol m^{-2} s^{-1})$^{-1}$)). The observation site in the figure is represented by a five-pointed star and the area surrounded by the red line is Beijing.

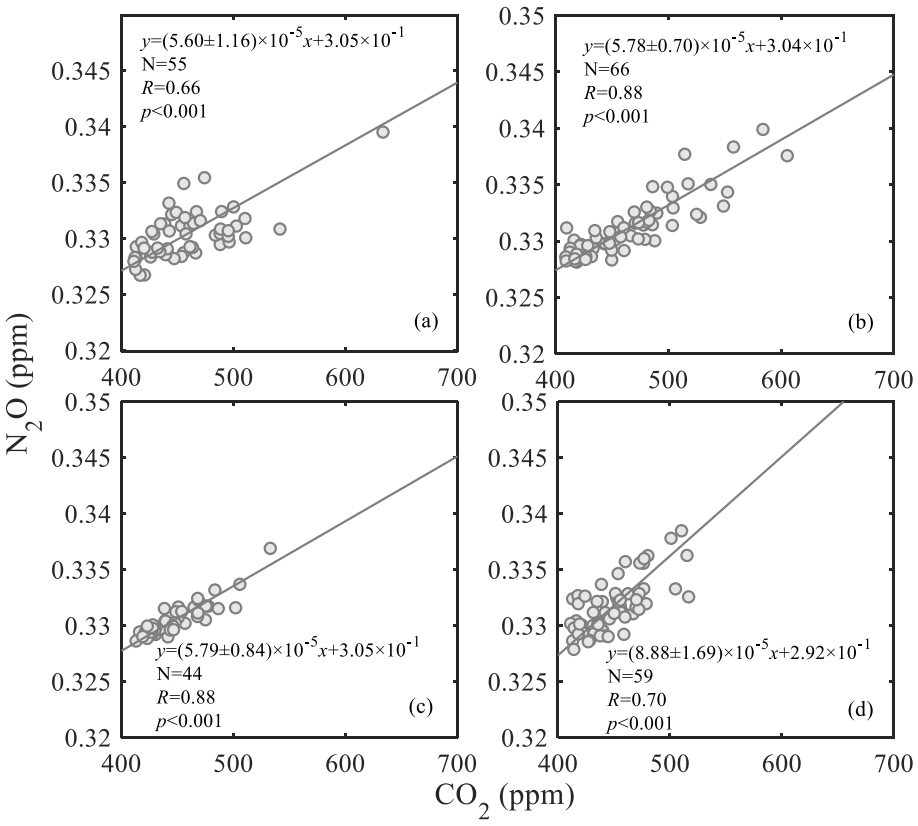

Fig. 6. Scatter plots of N_2O and CO_2 concentrations in (a) December 2015–February 2016; (b) December 2016–February 2017; (c) December 2017–February 2018; and (d) December 2018–February 2019 in Beijing from 2015 to 2018. Each data point represents one daytime mean value after wind direction selection (0–270°). Regression statistics (regression equation, linear correlation *R* and number of samples) are also shown.

sources, FFDAs provided the highest CO_2 emissions estimate at 1.63 × 10^8 t per year, followed by ODIAC at 1.60 × 10^8 t per year and EDGAR at 1.50 × 10^8 t per year, based on a 2015 case study. These inventories are based on provincial or national statistical data. In contrast, the GID model provided the lowest estimate for Beijing's CO_2 emissions, at 7.17 × 10^7 t per year in 2019, consistent with the inter-annual variation inferred from CEADs products. Regarding inter-annual trends, only the Beijing CO_2 emission estimates from NJU and CEADs indicated a decline between 2015 and 2019, while those from ODIAC, EDGAR, and MEIC indicated an increasing trend (Fig. 8).

Since the CEADs product incorporates locally optimized emission factors for China (Han et al., 2020c) and shows lower uncertainty at the national scale compared to other datasets (Table 1), this study used CEADs' CO_2 emissions for Beijing as the reference. Additionally, the agreement between CEADs' results and the latest GID data partially validates the estimated values.

Utilizing the previously derived slope values and the CO_2 emissions estimated by CEADs, CH_4 and N_2O emissions were calculated using Equation (1). The corresponding CO_2 equivalent values were determined by converting using the 20-year global warming potentials (GWP-20, 273 for N_2O and 81 for CH_4) and the 100-year global warming potentials (GWP-100, 273 for N_2O and 28 for CH_4) as specified in the IPCC Sixth Assessment Report (Table 3). The proportion factors for winter CO_2 emissions relative to total emissions, presented in the table, were derived from monthly CO_2 emissions estimated by the MEIC product, which includes a temporal module for allocating annual emissions to monthly values and has received user endorsement (Sha et al., 2019). Since this product only covers data through the end of 2017, winter proportions for 2017 and 2018 were linearly extrapolated from the previous two years' data. Between 2015 and 2018, Beijing reduced anthropogenic CO_2 emissions by 4.35 × 10^6 t. The decline in winter CO_2-equivalent emissions, which totaled 1.47 × 10^6 t over the period, shows a linear trend corresponding to an average reduction of approximately 5.30 × 10^5 t per season.

4. Discussion

4.1. Seasonal changes in concentration

CO_2 and CH_4 concentrations in Beijing showed significant peaks during the winters of 2015 (December 2015 to February 2016) and 2016 (December 2016 to February 2017), reaching levels 42.97 ppm higher than those at SDZ, a suburban monitoring site. The occurrence of these unusually high winter concentrations decreased significantly between 2017 and 2020. Similarly, Li et al. (2020) reported an abnormal increase in $PM_{2.5}$, PM_{10}, SO_2, CO, and NO_2 concentrations during the winters preceding 2016 (2013–2016). From 2016 to 2019, this seasonal trend was significantly reduced. This finding aligns closely with previous studies, which demonstrated that replacing coal with natural gas or coal-based synthetic natural gas for heating in Beijing could reduce haze pollutants emissions and $PM_{2.5}$ concentration by 52 % (Li et al., 2016). Beyond the synergistic effects between $PM_{2.5}$ and CO_2, $PM_{2.5}$—a key haze-causing pollutant—can create a turbulence barrier effect. While $PM_{2.5}$ is also known to suppress photosynthesis, this impact is negligible during the winter in Beijing because most local plants are deciduous (He et al., 2023; Wang et al., 2002). During haze episodes, Beijing's CO_2 concentration becomes more susceptible to influences from neighboring cities such as Hebei and Tianjin, while the reduction in $PM_{2.5}$ levels diminishes the contribution of regional transport to CO_2 levels (Feng et al., 2019). Given the distinct mechanisms of haze in summer and winter, severe haze in summer still permits good vertical diffusion conditions (Li et al., 2022).

The COVID-19 pandemic also exerted a notable influence on the variations of CO_2 and CH_4 concentrations in Beijing, while its impact on

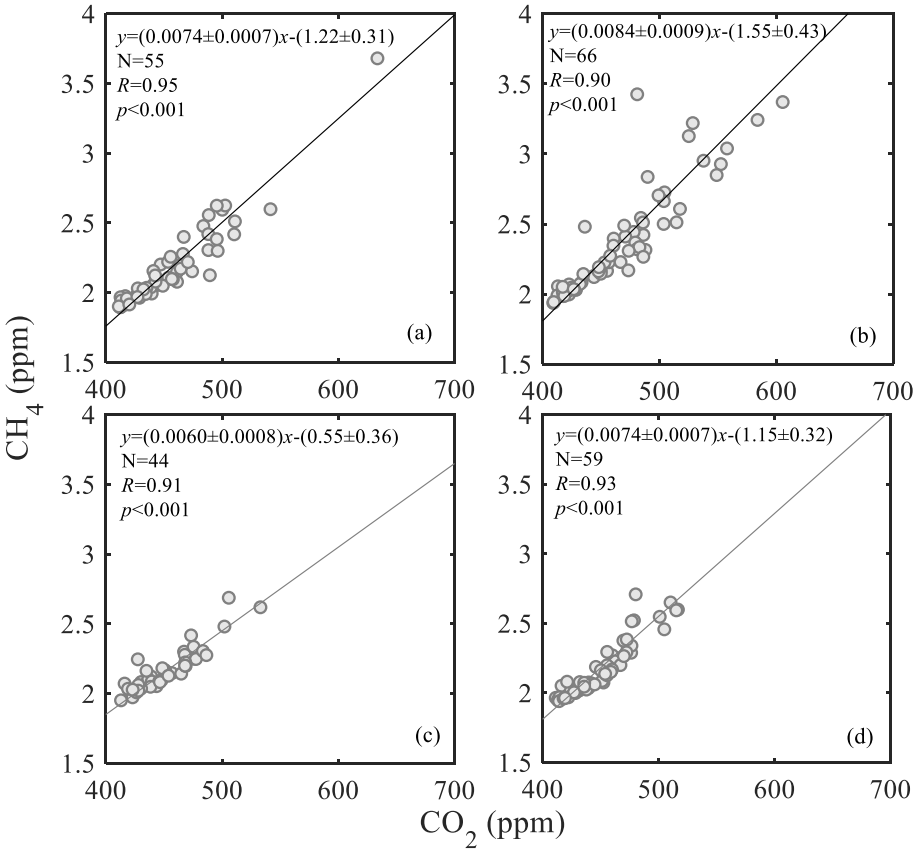

Fig. 7. Scatter plots of winter (December–February) daytime CH_4 and CO_2 concentrations in Beijing from 2015 to 2018. Other settings are the same as Fig. 7.

Table 2
Summary of CH_4/CO_2 and N_2O/CO_2 at different time scales and wind directions (WD).

Time scale	Period	$Slope_{CH4/CO2}$ ($\times 10^{-3}$ ppm ppm^{-1})		$Slope_{N2O/CO2}$ ($\times 10^{-5}$ ppm ppm^{-1})	
		WD (0–360°)	WD (0–270°)	WD (0–360°)	WD (0–270°)
half-hourly (11:00–16:00)	Dec 2015–Feb 2016	7.8 ± 0.2 (R = 0.91)	8.2 ± 0.3 (R = 0.89)	6.1 ± 0.3 (R = 0.67)	6.1 ± 0.4 (R = 0.67)
	Dec 2016–Feb 2017	8.6 ± 0.3 (R = 0.89)	9.0 ± 0.3 (R = 0.86)	5.9 ± 0.2 (R = 0.88)	6.0 ± 0.2 (R = 0.87)
	Dec 2017–Feb 2018	7.4 ± 0.3 (R = 0.81)	7.7 ± 0.4 (R = 0.77)	5.5 ± 0.2 (R = 0.88)	5.6 ± 0.3 (R = 0.85)
	Dec 2018–Feb 2019	7.7 ± 0.2 (R = 0.86)	8.2 ± 0.4 (R = 0.84)	7.7 ± 0.4 (R = 0.59)	8.3 ± 0.5 (R = 0.68)
daily (11:00–16:00)	Dec 2015–Feb 2016	7.1 ± 0.5 (R = 0.96)	7.4 ± 0.7 (R = 0.95)	5.6 ± 0.9 (R = 0.69)	5.6 ± 1.2 (R = 0.66)
	Dec 2016–Feb 2017	8.0 ± 0.7 (R = 0.92)	8.4 ± 0.9 (R = 0.90)	5.7 ± 0.6 (R = 0.89)	5.8 ± 0.7 (R = 0.88)
	Dec 2017–Feb 2018	5.8 ± 0.5 (R = 0.92)	6.0 ± 0.8 (R = 0.91)	5.5 ± 0.5 (R = 0.90)	5.8 ± 0.8 (R = 0.88)
	Dec 2018–Feb 2019	6.9 ± 0.5 (R = 0.93)	7.4 ± 0.7 (R = 0.93)	8.1 ± 1.4 (R = 0.60)	8.9 ± 1.7 (R = 0.70)

N_2O was not significant. Satellite-based column CO_2 data indicated that XCO_2 levels in Beijing from March to May 2020 were significantly affected by the pandemic, with the most pronounced reduction observed in March (Zhang et al., 2021). In light of these data gaps in this study, the annual average CO_2 and CH_4 concentration for 2019–2020 was thus based on the available data from April to November. Analysis of this truncated dataset revealed a pronounced slowdown in the growth of both CH_4 and CO_2. While the concentration trend for CO_2 aligns with the emission changes reported by Laughner et al. (2021), the finding for CH_4 contrasts with the emission trend reported for China by McNorton et al. (2022)—a discrepancy potentially explained by Beijing's status as a non-coal-mining city and its documented decrease in traffic emissions during COVID-19 restrictions (Liu et al., 2016; Taking 2018 as the reference year, CH_4 concentrations in Beijing decreased by 1.7 % in 2019 and by 4.9 % in 2020. In contrast, an anomalous increase in CH_4 levels was recorded at the WLG during the same period. Previous studies have suggested that the rise in background CH_4 may be attributed primarily to increased natural emissions from sources such as wetlands and a reduction in the hydroxyl radical (OH) sink (Lan et al., 2021; Peng et al., 2022). In contrast, the decrease in Beijing's CH_4 concentration is primarily attributable to anthropogenic factors, particularly the reduction in transportation emissions during the pandemic. A similar pattern was reported in Hangzhou, another major Chinese city, further supporting the link between reduced human activity and declining CH_4 levels during this period (Qing et al., 2022).

Due to data gaps during COVID-19 period, our study could not estimate GHG emissions for this heating season. However, statistical data for 2020 reveal an approximately 8 % decrease in Beijing's total energy consumption compared to 2019 (Fig. S5), with petroleum accounting for 94 % of this reduction. Supporting this trend, satellite-based emission estimates for China show that CO_2 emissions from January to April 2020 fell by 11.5 % relative to the same period in 2019, though emissions later rebounded to pre-pandemic levels (Zheng et al., 2020). These findings underscore the substantial yet transient impact of lockdown measures on regional emissions, while also highlighting the limitation posed by the absence of continuous observational data during the initial pandemic phase for a complete seasonal assessment.

In addition, the accuracy of GHG measurements using Cavity Ring-

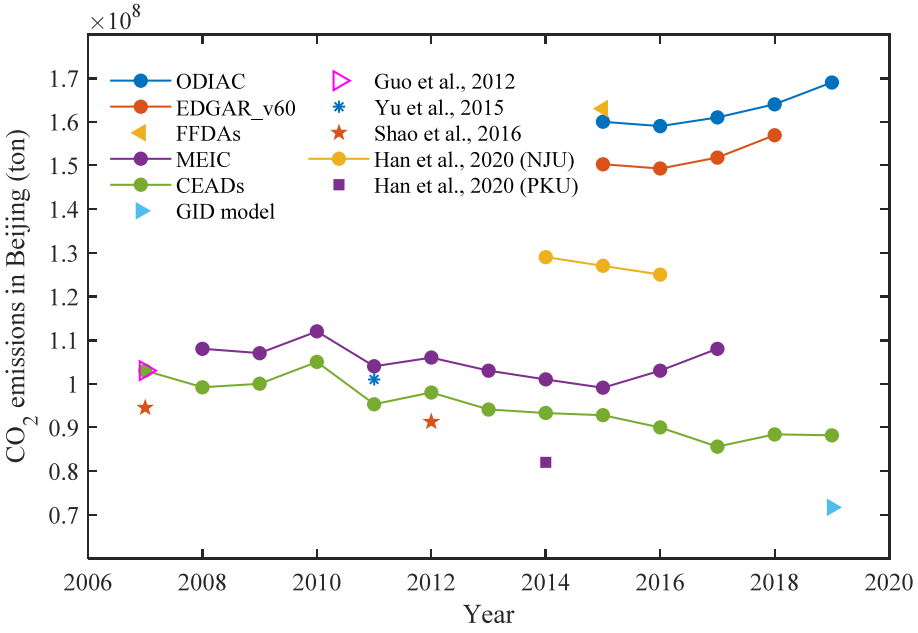

Fig. 8. Beijing CO_2 emissions based on inventory product estimates and previous research results.

Table 3
Estimation of CO_2, CH_4, N_2O emissions during a typical heating period (winter).

Description	2015 (ton)	2016 (ton)	2017 (ton)	2018 (ton)	2019
Estimated total anthropogenic CO_2 emission	9.28×10^7	9.00×10^7	8.56×10^7	8.84×10^7	8.82×10^7
Proportion of fuel use in winter (Dec, Jan, Feb)	0.109(2015), 0.228 (2016)	0.108(2016), 0.227 (2017)	0.108(2017), 0.224 (2018[a1])	0.107(2018[a1]), 0.222 (2019[a1])	
CO_2 emissions in winter	3.06×10^7	2.91×10^7	2.90×10^7	2.91×10^7	
N_2O emissions in winter	1.71×10^3	1.69×10^3	1.68×10^3	2.58×10^3	
CH_4 emissions in winter	8.28×10^4	8.89×10^4	6.36×10^4	7.82×10^4	
$CO_{2,eq\text{-}100}$ emissions in winter	3.34×10^7	3.21×10^7	3.13×10^7	3.20×10^7	
$CO_{2,eq\text{-}20}$ emissions in winter	3.78×10^7	3.68×10^7	3.47×10^7	3.62×10^7	

[a] [1]Indicates that the data is not directly obtained, but extrapolated.

Down Spectroscopy is subject to water vapor influence due to the absence of a drying system, an effect that has been noted and discussed here. First, under the low-H_2O conditions prevalent in winter (<5000 ppm)—the focus of our analysis, residual biases after applying the standard correction have been shown to exceed WMO compatibility thresholds in some cases, but are substantially smaller than the anthropogenic-emission-driven concentration variations that dominate the urban signals (Fig. S6, Rella et al., 2013; Reum et al., 2019; Stavert et al., 2019). Second, regarding the influence of prolonged dry calibration gas measurements, the shorter calibration sequence adopted in this study helps mitigate the short-term measurement bias associated with residual cavity moisture (Yver-Kwok et al., 2021). Therefore, the influence of water vapor on the reported data and subsequent analysis is considered negligible.

4.2. N_2O/CO_2, CH_4/CO_2 from different regions and energy types

The uncertainties of the CH_4/CO_2 and N_2O/CO_2 ratios ranged from 9.5 % to 13.3 % and 12.1 %–20.7 %, respectively. These results further support for the conclusion that the influence of residual water-vapor error on concentration measurements is negligible in comparison. The summary of slope values between concentrations is presented in Table 4. The CH_4/CO_2 ratios in this study, ranging from 6.0 to 8.4 ppb/ppm, are higher than that of the Nanjing suburb (4.3 ± 0.7 ppb/ppm) but lower than the ratios observed in Alaska and Canada. This discrepancy is likely due to the presence of extensive wetlands in Alaska and Canada, which contribute to elevated CH_4/CO_2 values. These high-latitude areas possess extensive wetlands, enhancing CH_4 emissions (Conway and Steele, 1989; Worthy et al., 1994). In contrast, the Nanjing suburb's location near an industrial park results in a dominance of CO_2-emitting activities (Shen et al., 2014).

Our study's observed N_2O/CO_2 ratios are lower than those reported in other studies. The elevated ratio in Pasadena, Los Angeles is largely due to agricultural land and forests, which account for over 60 % of the total N_2O emissions (Wunch et al., 2009). The high N_2O/CO_2 ratio in Edinburgh, Scotland, and the UK is primarily due to traffic emissions, which are a major source of N_2O in these regions. The N_2O/CO_2 ratio from cars with catalytic converters is ten times higher than that from cars without such devices. Haszpra et al. (2019) noted that the EDGAR products, when combined with trajectory analysis, fail to fully explain this discrepancy, highlighting the need for more detailed activity data and refined footprint analysis.

Fig. 9 summarizes the emission ratios of N_2O/CO_2 and CH_4/CO_2 from various energy sources. The emission coefficients were derived using emission factors from Ren et al. (2012) and Ge et al. (2016). In Beijing, reducing or eliminating coal use, along with increasing the share of natural gas in domestic energy consumption, was expected to modestly decrease the N_2O/CO_2 ratio and enhance the inter-annual trend of the CH_4/CO_2 ratio. However, this expectation contrasts sharply with the observed results for N_2O/CO_2 and does not explain the fluctuations in the CH_4/CO_2 ratio (Fig. S5). Consequently, changes in the coal and natural gas consumption structure cannot fully explain these phenomena. This suggests that additional emission sources contribute to the interannual variations in the N_2O/CO_2 and CH_4/CO_2 ratios in

Table 4
Summary of the slopes of CH_4/CO_2 and N_2O/CO_2.

Site	Period	CH_4/CO_2 (ppb/ppm)	N_2O/CO_2 ($\times 10^{-2}$ ppb/ppm)	References
Boulder, Colorado	Dec 1985	7.6 ± 0.7		Conway and Steele (1989)
Barrow, Alaska	Mar 1986	21.2 ± 0.4		
Barrow, Alaska	Apr 1986	13.5 ± 0.9		
Alert, North-West Territories, Canada	Apr 1986	20		Trivett et al. (1989)
Ocean Station "M"	1983–1989, winter	9.3 ± 1.7		
Barrow, Alaska	1989.03	11.0		Conway et al. (1993)
NOAA	1989–1990	9.14 ± 3.27		Jaffe et al. (1995)
Alert, NWT, Canada	Jan 1992–Apr 1992, black carbon >100 ng/m^3	13.0 ± 2.2		Worthy et al. (1994)
Black Forest, Germany	1991–1995, winter	4.8–9.9		Schmidt et al. (1996)
Ireland, western European pollution plume	1996	7.2	28	Biraud et al. (2000)
Barrow, Alaska	1986–1997, winter, nighttime	12.8 ± 0.3		Harris et al. (2000)
High Tatras, European mountain site	Jan, Feb, Dec 1997	9.5–11.7		Necki et al. (2003)
Pasadena, Los Angeles	Aug 2007–Jun 2008	7.8 ± 0.8	50 ± 30	Wunch et al. (2009)
Edinburgh, Scotland, UK	8 Nov – 19 Dec 2005		25.3	Famulari et al. (2010)
Los Angeles	Jun 2008	6.74 ± 0.58		Wennberg et al. (2012)
Los Angeles	May 2010–Jun 2010	6.55–6.7		Peischl et al. (2013)
Pasadena, Los Angeles	Sep 2011–Oct 2013	5.30–7.3		Wong et al. (2015)
NUIST, Nanjing, China	2010, winter, daytime	4.3 ± 0.7		Shen et al. (2014)
Alps, Germany, high mountain site	Oct 2012–Mar 2013	4.7–7.4		Ghasemifard et al. (2019)
MLW, Jiangsu, China	2012–2015, winter, daytime	5.5–7.5		Huang et al. (2019)
QJ, Anhui, China	2017, winter, daytime	6.1 ± 0.7		Huang et al. (2021)
Rural site, Pannonian Basin, Europe	Jan & Feb 2017, three cold-air pool episodes	6.7–13.8	15–31	Haszpra et al. (2019)
Beijing, China	Dec 2015–Feb 2019, winter, daytime	6.0–8.4	5.6–8.9	This study

Beijing. These processes include, but are not limited to, the chemical consumption of CH_4 by OH (Zhao et al., 2020), emissions from natural gas pipeline leakage (Wang et al., 2022), advancements in wastewater treatment processes (Zhou et al., 2022), and variations in the gas permeability and methane oxidation capacity of landfill cover layers, which are influenced by temperature, moisture, precipitation, and other factors (Li et al., 2020).

4.3. Inter-annual variations in winter greenhouse gas emission ratios post-heating reform

During the transition between heating energy types, it is important to investigate the correlation between the annual increase in natural gas consumption in Beijing and fluctuations in the CH_4/CO_2 ratio (Fig. S5). Additionally, identifying the primary factors contributing to the annual increase in the N_2O/CO_2 ratio during winter is crucial. Compared to the interannual emission ratios from the existing greenhouse gas inventory product (EDGAR V60), the observed CH_4/CO_2 values were lower than those estimated by EDGAR V60 (Table 5). The observed N_2O/CO_2 ratios closely matched the inventory estimations for 2016 and 2017. However, the N_2O/CO_2 emission ratios estimated by EDGAR V60 showed a decreasing trend over the years, in contrast to the observed values. Similarly, the CH_4/CO_2 emission ratios estimated by EDGAR V60 decreased annually, whereas the observed results did not show a clear interannual trend. Further analysis will examine the impact of fuel type usage, emission source contributions, oil quality, and traffic exhaust control measures to explain these discrepancies.

Analysis of the emission sources in Beijing using the EDGAR v60 database revealed that significant contributors to CH_4 emissions, with CH_4/CO_2 emission ratios exceeding the observed values, include fuel exploitation (PRO), solid waste landfill (SWD_LDF), energy use in buildings (RCO), enteric fermentation (ENF), and wastewater treatment (WWT). Other sources, deemed negligible, showed CH_4/CO_2 emission ratios one to three orders of magnitude lower than those observed, or their individual emissions were one to six orders smaller. In a related study conducted at a municipal solid waste landfill site in Beijing, Li et al. (2020) employed the static chamber method to monitor two landfill cells with different coverage times. Their results showed that the average CH_4/CO_2 emission ratios for these two cells during winter were 1.39 ppm ppm^{-1} and 1.41 ppm ppm^{-1}, respectively. Their study further indicated that winter CH_4 emissions accounted for 60.4 %–84.4 % of the annual total from low-emission zones, and the proportion was 17.4 %–68.7 % from high-emission zones. The CH_4/CO_2 emission ratio for WWT was found to be 1.25×10^{-2} ppm ppm^{-1}, based on the CO_2 and CH_4 emission inventory for China's WWT facilities, which was developed using the emission factor approach for pollutant reduction (Yan et al., 2018).

In Beijing, natural gas consumption has increased, while coal mining, livestock rearing, and landfill volumes have decreased, with significant interannual variability. The increased use of natural gas, including emissions from fuel combustion in residential, commercial, and institutional settings (RCO), has contributed to a higher atmospheric CH_4/CO_2 emission ratio. Data from the EDGAR v60 database reveal that, using 2015 as a baseline, natural gas consumption increased by 11 % in 2016, while landfill volume surged by 45 %. Conversely, coal production (PRO) and livestock populations experienced significant reductions. Specifically, coal production decreased by 29 %, while cattle, sheep, and poultry declined by 8 %–14 %, with pig numbers remaining relatively stable. These combined factors resulted in a peak in CH_4/CO_2 values during winter 2016. The decrease in the CH_4/CO_2 ratio observed in winter 2017 is particularly noteworthy. In 2017, SWD_LDF increased by 34 % compared to 2015, a notable decrease from the 45 % rise in 2016. Moreover, PRO dropped by 43 %, and livestock numbers decreased by 27 %–49 % across cattle, sheep, pigs, and poultry. Furthermore, the growth in natural gas consumption in 2017 was modest, with a 14 % increase compared to 2015, and only a 3 % rise from the 11 % increase in 2016. It is hypothesized that the substantial reduction in livestock production, the continued decline in coal mining, and the stable trend in natural gas use are the primary factors behind the observed decrease in the CH_4/CO_2 slope during winter 2017. In 2018, natural gas consumption continued to rise, with a 25 % increase compared to 2015, in line with the annual growth trend observed in 2016. Consequently, the CH_4/CO_2 emission ratio in 2018 rebounded.

Similarly, sources with N_2O/CO_2 emission ratios exceeding the

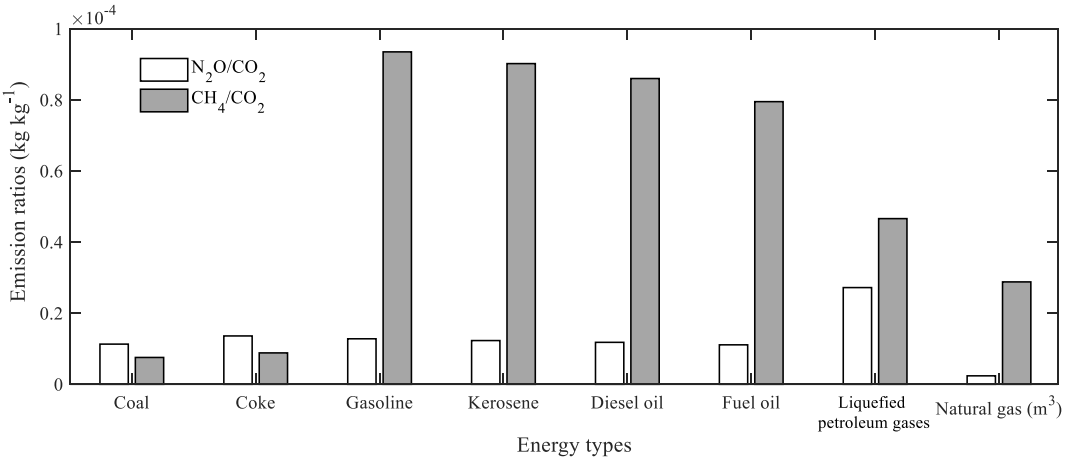

Fig. 9. N_2O/CO_2, CH_4/CO_2 emission ratios of different energy types.

Table 5
Emission ratios of CH_4 and N_2O to CO_2 during heating seasons in Beijing based on EDGAR v60 (units: ppm ppm^{-1}).

Year	EDGAR v60		This study (Observations)	
	N_2O/CO_2	CH_4/CO_2	N_2O/CO_2	CH_4/CO_2
2015	7.30×10^{-5}	1.15×10^{-2}	$(5.60 \pm 1.16) \times 10^{-5}$	$(7.44 \pm 0.67) \times 10^{-3}$
2016	5.36×10^{-5}	1.13×10^{-2}	$(5.78 \pm 0.70) \times 10^{-5}$	$(8.39 \pm 0.93) \times 10^{-3}$
2017	5.29×10^{-5}	1.09×10^{-2}	$(5.79 \pm 0.84) \times 10^{-5}$	$(6.02 \pm 0.79) \times 10^{-3}$
2018	–	–	$(8.88 \pm 1.69) \times 10^{-5}$	$(7.39 \pm 0.72) \times 10^{-3}$

observed values and significantly contributing to N_2O emissions include AGS, WWT, SWD_INC, manure management, indirect N_2O emissions from agriculture, and emissions from railways, pipelines, and off-road transport (TNR_Other). Given the negligible greenhouse gas emission potential of agricultural activities in winter, which is attributed to the limited proportion of agricultural land and the low N_2O emission factors of major crops such as wheat, corn, and vegetables (Bhandari et al., 2020; Yan et al., 2014), agricultural soils, indirect N_2O from agriculture, and manure management were excluded from this analysis.

Among the potential contributing sources mentioned—WWT, SWD_INC, and TNR_Other, WWT was identified as the largest emitter of N_2O. Given the increasing volume of wastewater in Beijing year by year, it is reasonable to predict that WWT is the primary driver of the observed annual increase in N_2O/CO_2 ratios. Research on greenhouse gas emissions from wastewater treatment in China has found that the N_2O/CO_2 emission ratio, excluding energy consumption in the WWT process, is 3.27×10^{-4} ppm ppm^{-1}. Additionally, N_2O emission levels are positively correlated with the local economic development (Yan et al., 2018). The N_2O/CO_2 emission ratio is one to two orders of magnitude higher than those of coal and natural gas. As a result, the impact of energy transition on the N_2O/CO_2 emission ratio can be mitigated, allowing the observed values to maintain an upward trend annually.

Estimating the impact of TNR_Other on the observed N_2O/CO_2 ratios over the years is challenging. On one hand, the emission ratio associated with the increased diesel and gasoline use aligns with the observed N_2O/CO_2 emission ratios from 2015 to 2019, although it is slightly lower than the actual observed values (Razif and Santoso, 2016). On the other hand, recent policy initiatives have led to improvements in fuel quality and vehicle exhaust treatment. In April 2016, all diesel and gasoline vehicles in Beijing were required to comply with the National Fifth standard, and the use of three-way catalysts became more widespread for treating motor vehicle emissions, including nitrogen oxides and hydrocarbons. Initially, the deployment of three-way catalysts increased N_2O emissions, which were found to rise with the catalysts' service life. However, the development of newer catalysts has facilitated more effective removal of volatile organic compounds, resulting in a decrease in N_2O emissions (Graham et al., 2008; Wallington and Wiesen, 2014). Nevertheless, compared to Euro 5 and pre-Euro IV standards for L-category vehicles in the European Union, higher-standard diesel vehicles exhibit higher N_2O emissions, likely due to the implementation of after-treatment systems to meet more stringent NO_x emission standards (Clairotte et al., 2020). Furthermore, as of January 2017, gasoline and diesel meeting the fifth national standard were supplied nationwide, and by the end of September 2017, Beijing had fully transitioned to gasoline and diesel meeting the national VI standards.

In summary, the findings above are benchmarked against a comparison of inventory outputs and observed mole fraction ratios of different gases. Future research could incorporate isotopic methods to constrain emission source apportionment from an additional observational dimension. For instance, a study in Nanjing analyzing atmospheric CO_2 mole fractions and $\delta^{13}C$ isotopic composition successfully distinguished and quantified anthropogenic versus natural carbon emissions in the Yangtze River Delta region (Xu et al., 2017). In another example, stable isotopic approaches were applied to quantify N_2O emissions and source attribution under different irrigation management practices (Ding et al., 2019). Furthermore, airborne observations downwind of the North Sea gas fields utilized three distinct methods—a mass balance method, atmospheric dispersion model, and isotopic analysis, highlighting that supplementing mole fraction measurements with isotopic data can significantly reduce misattribution of emission sources (Cain et al., 2017).

5. Conclusions

This study focused on Beijing, a city undergoing significant energy structure transformation, particularly with notable success in phasing out coal. CO_2, CH_4, and N_2O concentrations were monitored from 2015 to 2020. Employing a top-down approach, CO_2 used as a tracer to estimate emissions of CH_4 and N_2O from anthropogenic activities during the winter heating season. Consequently, the anthropogenic greenhouse gas emissions and their interannual trends in Beijing were determined. The main findings are summarized below:

First, the transformation of Beijing's energy structure has not only reduced $PM_{2.5}$ concentrations and haze episodes but also indirectly influenced the seasonal trends of greenhouse gas concentrations. Second, while the CH_4/CO_2 emission ratio in Beijing is consistent with that observed in other regions, the N_2O/CO_2 emission ratio is notably lower than values reported in previous studies. In terms of emission

reductions, the shift in energy structure has led to a direct decrease in greenhouse gas emissions, with an average annual reduction of 5.30 × 10^5 t of CO_2-equivalent emissions during winter between 2015 and 2018. Finally, analysis of emission ratio dynamics revealed that the observed CH_4/CO_2 ratio underwent three distinct phases: an initial increase, followed by a decline, and a subsequent rebound. The decrease in 2017 was mainly driven by a sharp reduction in livestock production, a continued decline in coal mining, and stabilized natural gas consumption. In addition, interannual variations in the N_2O/CO_2 emission ratio during the heating season were primarily influenced by wastewater handling, which had a more significant impact than changes in energy infrastructure—a finding not yet reflected in current emission inventory products. Future integration of concentration data with isotopic measurements will enhance our ability to constrain source apportionment.

Our measurements, conducted without a drying system, do not comply with the strict standard operating procedures of high-precision networks such as ICOS, and therefore the data should be interpreted accordingly in concentration-based evaluations. Future improvements to meet such standards would require the implementation of a drying system or more advanced water-vapor correction models. Also, we acknowledge that the absence of data during the initial COVID-19 lockdown period (December 2019–March 2020) limits our ability to evaluate short-term emission responses during a historically significant disruption. Finally, this study estimated only direct emissions within the city (Scope 1 in inventory compilation), facilitating comparison with model inversion studies. However, Beijing's energy structure transformation, in addition to increased natural gas usage, also involves importing electricity generated from other regions, thus ignoring emissions in Scope 2 and 3. At the national scale, it cannot serve as a guiding case for structural transformation of sources.

CRediT authorship contribution statement

Wenjing Huang: Writing – review & editing, Writing – original draft, Methodology, Investigation. **Wei Xiao:** Writing – review & editing, Supervision, Funding acquisition. **Xuefa Wen:** Resources, Data curation. **Jie Wei:** Resources, Data curation. **Sidan Lyu:** Resources, Data curation. **Cheng Hu:** Writing – review & editing, Validation, Methodology. **Mi Zhang:** Resources, Project administration, Investigation. **Ning Hu:** Resources, Methodology. **Xuhui Lee:** Supervision, Methodology, Conceptualization.

Declaration of competing interest

The authors declare that they have no known competing financial interests or personal relationships that could have appeared to influence the work reported in this paper.

Acknowledgments

This work was supported by the Jing-Jin-Ji Regional Integrated Environmental Improvement-National Science and Technology Major Project, Ministry of Ecology and Environment, China (2025ZD1200903), the National Natural Science Foundation, China (U24A20590, 42021004), and the "333 Project" of Jiangsu Province, China (BRA2022023).

Appendix A. Supplementary data

Supplementary data to this article can be found online at https://doi.org/10.1016/j.apr.2025.102861.

References

Allen, M.R., Peters, G.P., Shine, K.P., Azar, C., Balcombe, P., Boucher, O., Cain, M., Ciais, P., Collins, W., Forster, P.M., Frame, D.J., Friedlingstein, P., Fyson, C., Gasser, T., Hare, B., Jenkins, S., Hamburg, S.P., Johansson, D.J.A., Lynch, J., Macey, A., Morfeldt, J., Nauels, A., Ocko, I., Oppenheimer, M., Pacala, S.W., Pierrehumbert, R., Rogelj, J., Schaeffer, M., Schleussner, C.F., Shindell, D., Skeie, R. B., Smith, S.M., Tanaka, K., 2022. Indicate separate contributions of long-lived and short-lived greenhouse gases in emission targets. npj Clim. Atmos. Sci. 5 (1), 1–5. https://doi.org/10.1038/s41612-021-00226-2.

Archer, D., Brovkin, V., 2008. The millennial atmospheric lifetime of anthropogenic CO_2. Clim. Change 90 (3), 283–297.

Asefi-Najafabady, S., Rayner, P.J., Gurney, K.R., McRobert, A., Song, Y., Coltin, K., Huang, J., Elvidge, C., Baugh, K., 2014. A multiyear, global gridded fossil fuel CO_2 emission data product: evaluation and analysis of results. J. Geophys. Res. Atmos. 119, 10213–10231. https://doi.org/10.1002/2013JD021296.

Baldocchi, D., Falge, E., Gu, L., Olson, R., Hollinger, D., Running, S., Anthoni, P., Bernhofer, Ch, Davis, K., Evans, R., Fuentes, J., Goldstein, A., Katul, G., Law, B., Lee, X., Malhi, Y., Meyers, T., Munger, W., Oechel, W., Paw U, K.T., Pilegaard, K., Schmid, H.P., Valentini, R., Verma, S., Vesala, T., Wilson, K., Wofsy, S., 2001. FLUXNET: a new tool to study the temporal and spatial variability of ecosystem-scale carbon dioxide, water vapor, and energy flux densities. Bull. Am. Meteorol. Soc. 82 (11), 2415–2434.

Bhandari, M., Ma, Y., Men, M., Wu, M., Xue, C., Wang, Y., Li, Y., Peng, Z., 2020. Response of winter wheat yield and soil N_2O emission to nitrogen fertilizer reduction and nitrapyrin application in North China Plain. Commun. Soil Sci. Plant Anal. 51 (4), 554–565.

Biraud, S., Ciais, P., Ramonet, M., Simmonds, P., Kazan, V., Monfray, P., O'Doherty, S., Spain, T.G., Jennings, S.G., 2000. European greenhouse gas emissions estimated from continuous atmospheric measurements and radon 222 at Mace Head, Ireland. J. Geophys. Res. Atmos. 105 (D1), 1351–1366.

Brunke, E.G., Ebinghaus, R., Kock, H.H., Labuschagne, C., Slemr, F., 2012. Emissions of mercury in Southern Africa derived from long-term observations at Cape Point, South Africa. Atmos. Chem. Phys. 12 (16), 7465–7474.

Cai, B., Liang, S., Zhou, J., Wang, J., Cao, L., Qu, S., Xu, M., Yang, Z., 2018. China high resolution emission database (CHRED) with point emission sources, gridded emission data, and supplementary socioeconomic data. Resources, Resour. Conserv. Recycl. 129, 232–239. https://doi.org/10.1016/j.resconrec.2017.10.036.

Cain, M., Warwick, N.J., Fisher, R.E., Lowry, D., Lanoiselle, M., Nisbet, E.G., France, J., Pitt, J., O'Shea, S., Bower, K.N., Allen, G., Ilingworth, S., Manning, A.J., Bauguitte, S., Pisso, I., Pyle, J.A., 2017. A cautionary tale: a study of a methane enhancement over the North Sea. J. Geophys. Res. Atmos. 122, 7630–7645. https://doi.org/10.1002/2017JD026626.

Chen, G., Zhang, B., 2010. Greenhouse gas emissions in China 2007: inventory and input–output analysis. Energy Policy 38 (10), 6180–6193.

Chen, J., Zhao, F., Zeng, N., Oda, T., 2020. Comparing a global high-resolution downscaled fossil fuel CO_2 emission dataset to local inventory-based estimates over 14 global cities. Carbon Bal. Manag. 15, 1–15.

Chen, Y., Prinn, R.G., 2006. Estimation of atmospheric methane emissions between 1996 and 2001 using a three-dimensional global chemical transport model. J. Geophys. Res. Atmos. 111 (D10), 1–25. https://doi.org/10.1029/2005JD006058.

Chen, Z., Griffis, T.J., Millet, D.B., Wood, J.D., Lee, X., Baker, J.M., Xiao, K., Turner, P.A., Chen, M., Wells, K.C., 2016. Partitioning N_2O emissions within the US corn belt using an inverse modeling approach. Glob. Biogeochem. Cycles 30, 1192–1205.

Ciais, P., Sabine, C., Bala, G., Bopp, L., Brovkin, V.E., House, J.I., 2014. Carbon and other biogeochemical cycles. In: Stocker, T.F., et al. (Eds.), Climate Change 2013: the Physical Science Basis. Contribution of Working Group I to the Fifth Assessment Report of the Intergovernmental Panel on Climate Change. Cambridge University Press, Cambridge, pp. 465–570.

Clairotte, M., Suarez-Bertoa, R., Zardini, A.A., Giechaskiel, B., Pavlovic, J., Valverde, V., Ciuffo, B., Astorga, C., 2020. Exhaust emission factors of greenhouse gases (GHGs) from European road vehicles. Environ. Sci. Eur. 32 (125), 1–20. https://doi.org/10.1186/s12302-020-00407-5.

Conway, T.J., Steele, L.P., Novelli, P.C., 1993. Correlations among atmospheric CO_2, CH_4 and CO in the Arctic, March 1989. Atmos. Environ., Part A 27 (17–18), 2881–2894.

Conway, T.J., Steele, L.P., 1989. Carbon dioxide and methane in the Arctic atmosphere. J. Atmos. Chem. 9 (1), 81–99.

Dai, H., Mischke, P., Xie, X., Xie, Y., Masui, T., 2016. Closing the gap? top-down versus bottom-up projections of China's regional energy use and CO_2 emissions. Appl. Energy 162, 1355–1373. https://doi.org/10.1016/j.apenergy.2015.06.069.

Ding, J., Fang, F., Lin, W., Qiang, X., Xu, C., Mao, L., Li, Q., Zhang, X., Li, Y., 2019. N_2O emissions and source partitioning using stable isotopes under furrow and drip irrigation in vegetable field of North China. Sci. Total Environ. 665, 709–717.

Dlugokencky, E.J., Nisbet, E.G., Fisher, R.E., Lowry, D., 2011. Global atmospheric methane: budget changes and dangers. Philos. Trans. R. Soc. A 369 (1943), 2058–2072. https://doi.org/10.1098/rsta.2010.0341.

EPA, 2012. Global Anthropogenic non-CO_2 Greenhouse Gas Emissions, pp. 1990–2030.

Famulari, D., Nemitz, E., Di Marco, C., Phillips, G.J., Thomas, R., House, E., Fowler, D., 2010. Eddy-covariance measurements of nitrous oxide fluxes above a city. Agric. For. Meteorol. 150 (6), 786–793.

Feng, T., Zhou, W., Wu, S., Niu, Z., Cheng, P., Xiong, X., Li, G., 2019. High-resolution simulation of wintertime fossil fuel CO_2 in Beijing, China: characteristics, sources, and regional transport. Atmos. Environ. 198, 226–235.

Galloway, J.N., Townsend, A.R., Erisman, J.W., Bekunda, M., Cai, Z., Freney, J.R., Martinelli, L.A., Seitzinger, S.P., Sutton, M.A., 2008. Transformation of the nitrogen cycle: recent trends, questions, and potential solutions. Science 320 (5878), 889–892. https://doi.org/10.1126/science.1136674.

Gerbig, C., Lin, J.C., Wofsy, S.C., Daube, B.C., Andrews, A.E., Stephens, B.B., Bakwin, P. S., Grainger, C.A., 2003a. Toward constraining regional-scale fluxes of CO_2 with atmospheric observations over a continent: 1. Observed spatial variability from

airborne platforms. J. Geophys. Res. Atmos. 108 (D24), 1–14. https://doi.org/10.1029/2002JD003018.
Gerbig, C., Lin, J.C., Wofsy, S.C., Daube, B.C., Andrews, A.E., Stephens, B.B., Bakwin, P. S., Grainger, C.A., 2003b. Toward constraining regional-scale fluxes of CO_2 with atmospheric observations over a continent: 2. Analysis of COBRA data using a receptor-oriented framework. J. Geophys. Res. Atmos. 108 (D24), 1–27. https://doi.org/10.1029/2003JD003770.
Ghasemifard, H., Vogel, F.R., Yuan, Y., Luepke, M., Chen, J., Ries, L., Leuchner, M., Schunk, C., Vardag, S.N., Menzel, A., 2019. Pollution events at the high-altitude mountain site Zugspitze-Schneefernerhaus (2670 m asl), Germany. Atmosphere 10 (6), 1–17.
Gong, P., Liu, H., Zhang, M., Li, M., Wang, J., Huang, H., Clinton, N., Ji, L.W., Bai, Y., Chen, B., Xu, B., Zhu, Z., Yuan, C., Suen, H.P., Guo, J., Xu, N., Li, W., Zhao, Y., Yang, J., Yu, C., Wang, X., Fu, H., Yu, L., Dronova, I., Hui, F., Cheng, X., Shi, X., Xiao, F., Liu, Q., Song, L., 2019. Stable classification with limited sample: transferring a 30-m resolution sample set collected in 2015 to mapping 10-m resolution global land cover in 2017. Sci. Bull. 64 (6), 370–373. https://doi.org/10.1016/j.scib.2019.03.002.
Graham, L.A., Rideout, G., Rosenblatt, D., Hendren, J., 2008. Greenhouse gas emissions from heavy-duty vehicles. Atmos. Environ. 42 (19), 4665–4681. https://doi.org/10.1016/j.atmosenv.2008.01.049.
Guan, D., Meng, J., Reiner, D.M., Zhang, N., Shan, Y., Mi, Z., Shao, S., Liu, Z., Zhang, Q., Davis, S.J., 2018. Structural decline in China's CO_2 emissions through transitions in industry and energy systems. Nat. Geosci. 11 (8), 551–555.
Han, P., Zeng, N., Oda, T., Lin, X., Crippa, M., Guan, D., Janssens-Maenhout, G., Ma, X., Liu, Z., Shan, Y., Tao, S., Wang, H., Wang, R., Wu, L., Yun, X., Zhang, Q., Zhao, F., Zheng, B., 2020a. Evaluating China's fossil-fuel CO_2 emissions from a comprehensive dataset of nine inventories. Atmos. Chem. Phys. 20 (19), 11371–11385. https://doi.org/10.5194/acp-20-11371-2020.
Han, P., Zeng, N., Oda, T., Zhang, W., Lin, X., Liu, D., Cai, Q., Ma, X., Meng, W., Wang, G., Zheng, B., 2020b. A city-level comparison of fossil-fuel and industry processes-induced CO_2 emissions over the Beijing-Tianjin-Hebei region from eight emission inventories. Carbon Bal. Manag. 15 (25), 1–16. https://doi.org/10.1186/s13021-020-00163-2.
Han, P., Lin, X., Zeng, N., Oda, T., Zhang, W., Liu, D., Cai, Q., Crippa, M., Guan, D., Ma, X., Janssens-Maenhout, G., Meng, W., Shan, Y., Tao, S., Wang, G., Wang, H., Wang, R., Wu, L., Zhang, Q., Zhao, F., Zheng, B., 2020c. Province-level fossil fuel CO_2 emission estimates for China based on seven inventories. J. Clean. Prod. 277. https://doi.org/10.1016/j.jclepro.2020.123377. Article 123377.
Harris, J.M., Dlugokencky, E.J., Oltmans, S.J., Conway, T.J., Novelli, P.C., Thoning, K. W., 2000. An interpretation of trace gas correlations during Barrow, Alaska, winter dark periods, 1986–1997. J. Geophys. Res. Atmos. 105 (D13), 17267–17278.
Haszpra, L., Ferenczi, Z., Barcza, Z., 2019. Estimation of greenhouse gas emission factors based on observed covariance of CO_2, CH_4, N_2O and CO mole fractions. Environ. Sci. Eur. 31 (95), 1–12. https://doi.org/10.1186/s12302-019-0277-y.
He, L., Rosa, L., Lobell, D.B., Wang, Y., Yin, Y., Doughty, R., Yao, Y., Berry, J.A., Frankenberg, C., 2023. The weekly cycle of photosynthesis in Europe reveals the negative impact of particulate pollution on ecosystem productivity. Proc. Natl. Acad. Sci. USA 120 (49), e2306507120.
Hu, C., Griffis, T.J., Lee, X., Millet, D.B., Chen, Z., Baker, J.M., Xiao, K., 2018a. Top-down constraints on anthropogenic CO_2 emissions within an agricultural-urban landscape. J. Geophys. Res. Atmos. 123, 4674–4694. https://doi.org/10.1029/2017JD027881.
Hu, C., Liu, S., Wang, Y., Zhang, M., Xiao, W., Wang, W., Xu, J., 2018b. Anthropogenic CO_2 emissions from a megacity in the Yangtze River Delta of China. Environ. Sci. Pollut. Res. 25 (23), 23157–23169. https://doi.org/10.1007/s11356-018-2325-3.
Huang, W., Griffis, T.J., Hu, C., Xiao, W., Lee, X., 2021. Seasonal variations of CH_4 emissions in the Yangtze River Delta region of China are driven by agricultural activities. Adv. Atmos. Sci. 38 (9), 1537–1551.
Huang, W., Xiao, W., Zhang, M., Wang, W., Xu, J., Hu, Y., Hu, C., Liu, S., Lee, X., 2019. Anthropogenic CH_4 emissions in the Yangtze River Delta based on a "Top-Down" method. Atmosphere 10 (4), 1–21.
IPCC, 2021. Climate Change 2021: the Physical Science Basis. Contribution of Working Group I to the Sixth Assessment Report of the Intergovernmental Panel on Climate Change. Cambridge University Press.
Jaffe, D.A., Honrath, R.E., Furness, D., Conway, T.J., Dlugokencky, E., Steele, L.P., 1995. A determination of the CH_4, NO_x and CO_2 emissions from the Prudhoe Bay, Alaska oil development. J. Atmos. Chem. 20 (3), 213–227.
Jaffe, D., Prestbo, E., Swartzendruber, P., Weiss-Penzias, P., Kato, S., Takami, A., Hatakeyama, S., Kajii, Y., 2005. Export of atmospheric mercury from Asia. Atmos. Environ. 39 (17), 3029–3038. https://doi.org/10.1016/j.atmosenv.2005.01.030.
Janssens-Maenhout, G., Crippa, M., Guizzardi, D., Muntean, M., Schaaf, E., Dentener, F., Bergamaschi, P., Pagliari, V., Olivier, J.G.J., Peters, J.A.H.W., van Aardenne, J.A., Monni, S., Doering, U., Petrescu, A.M.R., Solazzo, E., Oreggioni, G.D., 2019. EDGAR v4.3.2 global atlas of the three major greenhouse gas emissions for the period 1970–2012. Earth Syst. Sci. Data 11 (3), 959–1002. https://doi.org/10.5194/essd-11-959-2019.
Kurosawa, A., 2006. Multigas mitigation: an economic analysis using GRAPE model. Energy J. 27 (3), 275–288.
Lan, X., Nisbet, E.G., Dlugokencky, E.J., Michel, S.E., 2021. What do we know about the global methane budget? Results from four decades of atmospheric CH_4 observations and the way forward. Phil. Trans. R. Soc. A 379 (2210), 20200440.
Laughner, J.L., Neu, J.L., Schimel, D., Wennberg, P.O., Barsanti, K., Bowman, K.W., Chatterjee, A., Croes, B.E., Fitzmaurice, H.L., Henze, D.K., Kim, J., Kort, E.A., Liu, Z., Miyazaki, K., Turner, A.J., Anenberg, S., Avise, J., Cao, H., Crisp, D., de Gouw, J., Eldering, A., Fyfe, J.C., Goldberg, D.L., Gurney, K.R., Hasheminassab, S., Hopkins, F., Ivey, C.E., Jones, D.B.A., Liu, J., Lovenduski, N.S., Martin, R.V., McKinley, G.A., Ott, L., Poulter, B., Rubbo, M., Sander, S.P., Swart, N., Yung, Y.L., Zeng, Z.C., rest of the Keck Institute for Space Studies, 2021. "COVID-19: identifying Unique Opportunities for Earth System Science" study team. Societal shifts due to COVID-19 reveal large-scale complexities and feedbacks between atmospheric chemistry and climate change. Proc. Natl. Acad. Sci. USA 118 (46), e2109481118.
Lelieveld, J., Crutzen, P.J., Dentener, F.J., 1998. Changing concentration, lifetime and climate forcing of atmospheric methane. Tellus Ser. B Chem. Phys. Meteorol. 50, 128–150.
Li, H., Yang, S., Zhang, J., Qian, Y., 2016. Coal-based synthetic natural gas (SNG) for municipal heating in China: analysis of haze pollutants and greenhouse gases (GHGs) emissions. J. Clean. Prod. 112, 1350–1359.
Li, Q., Zhang, H., Jin, X., Cai, X., Song, Y., 2022. Mechanism of haze pollution in summer and its difference with winter in the North China Plain. Sci. Total Environ. 806, 1–9. https://doi.org/10.1016/j.scitotenv.2021.150625.
Li, W., Shao, L., Wang, W., Li, H., Wang, X., Li, Y., Li, W., Jones, T., Zhang, D., 2020. Air quality improvement in response to intensified control strategies in Beijing during 2013–2019. Sci. Total Environ. 744, 1–15. https://doi.org/10.1016/j.scitotenv.2020.140776.
Lin, J.C., Gerbig, C., Wofsy, S.C., Andrews, A.E., Daube, B.C., Davis, K.J., Grainger, C.A., 2003. A near-field tool for simulating the upstream influence of atmospheric observations: the stochastic time-inverted lagrangian transport (STILT) model. J. Geophys. Res. Atmos. 108 (D16), 1–18.
Liu, D., Sun, W., Zeng, N., Han, P., Yao, B., Liu, Z., Wang, P., Zheng, K., Mei, H., Cai, Q., 2021. Observed decreases in on-road CO_2 concentrations in Beijing during COVID-19. Atmos. Chem. Phys. 21, 4599–4614.
Liu, M., Wang, H., Oda, T., Zhao, Y., Yang, X., Zang, R., Zang, B., Bi, J., Chen, J., 2013. Refined estimate of China's CO_2 emissions in spatiotemporal distributions. Atmos. Chem. Phys. 13 (21), 10873–10882. https://doi.org/10.5194/acp-13-10873-2013.
Liu, M., Zhu, X., Pan, C., Chen, L., Zhang, H., Jia, W., Xiang, W., 2016. Spatial variation of near-surface CO_2 concentration during spring in Shanghai. Atmos. Pollut. Res. 7 (1), 31–39. https://doi.org/10.1016/j.apr.2015.07.002.
Liu, Z., Guan, D., Wei, W., Davis, S.J., Ciais, P., Bai, J., Peng, S., Zhang, Q., Hubacek, K., Marland, G., Andres, R.J., Crawford-Brown, D., Lin, J., Zhao, H., Hong, C., Boden, T. A., Feng, K., Peters, G.P., Xi, F., Liu, J., Li, Y., Zhao, Y., Zeng, N., He, K., 2015. Reduced carbon emission estimates from fossil fuel combustion and cement production in China. Nature 524 (7565), 335–338.
Mallia, D., Mitchell, L.E., Kunik, L., Fasoli, B., Bares, R., Gurney, K.R., Mendoza, D.L., Lim, J.C., 2020. Constraining urban CO_2 emissions using mobile observations from a light rail public transit platform. Environ. Sci. Technol. 54 (24), 15613–15621.
McNorton, J., Bousserez, N., Agustí-Panareda, A., Balsamo, G., Engelen, R., Huijnen, V., Inness, A., Kipling, Z., Parrington, M., Ribas, R., 2022. Quantification of methane emissions from hotspots and during COVID-19 using a global atmospheric inversion. Atmos. Chem. Phys. 22, 5961–5981.
Meurer, K., Franko, U., Spott, O., Stange, C.F., Jungkunst, H.F., 2016. Model testing for nitrous oxide (N_2O) fluxes from Amazonian cattle pastures. Atmos. Environ. 143, 67–78. https://doi.org/10.1016/j.atmosenv.2016.08.047.
Munger, J.W., Wang, S., Nielsen, C., McElroy, M.B., 2020. CO_2 and CH_4 observations surrounding Beijing to distinguish possible emission processes and locations. In: EGU General Assembly Conference Abstracts, 11858.
Necki, J., Schmidt, M., Rozanski, K., Zimnoch, M., Korus, A., Lasa, J., Graul, R., Levin, I., 2003. Six-year record of atmospheric carbon dioxide and methane at a high-altitude mountain site in Poland. Tellus B 55 (2), 94–104. https://doi.org/10.3402/tellusb.v55i2.16763.
Nisbet, E.G., Fisher, R.E., Lowry, D., France, J.L., Allen, G., Bakkaloglu, S., Broderick, T. J., Cain, M., Coleman, M., Fernandez, J., Forster, G., Griffiths, P.T., Iverach, C.P., Kelly, B.F.J., Manning, M.R., Nisbet-Jones, P.B.R., Pyle, J.A., Townsend-Small, A., al-Shalaan, A., Warwick, N., Zazzeri, G., 2020. Methane mitigation: methods to reduce emissions, on the path to the Paris agreement. Rev. Geophys. 58 (1) e2019RG000675.
Oda, T., Maksyutov, S., Andres, R.J., 2018. The open-source Data inventory for anthropogenic CO_2, version 2016 (ODIAC2016): a global monthly fossil fuel CO_2 gridded emissions data product for tracer transport simulations and surface flux inversions. Earth Syst. Sci. Data 10 (1), 87–107. https://doi.org/10.17595/20170411.001.
Peischl, J., Ryerson, T.B., Brioude, J., Aikin, K.C., Andrews, A.E., Atlas, E., Blake, D., Daube, B.C., de Gouw, J.A., Dlugokencky, E., Frost, G.J., Gentner, D.R., Gilman, J.B., Goldstein, A.H., Harley, R.A., Holloway, J.S., Kofler, J., Kuster, W.C., Lang, P.M., Novelli, P.C., Santoni, G.W., Trainer, M., Wofsy, S.C., Parrish, D.D., 2013. Quantifying sources of methane using light alkanes in the Los Angeles basin, California. J. Geophys. Res. Atmos. 118 (10), 4974–4990. https://doi.org/10.1002/jgrd.50413.
Peng, S., Lin, M., Thompson, R.L., Xi, Y., Liu, G., Hauglustaine, D., Lan, X., Poulter, B., Ramonet, M., Saunois, M., Yin, Y., Zhang, Z., Zheng, B., Ciais, P., 2022. Wetland emission and atmospheric sink changes explain methane growth in 2020. Nature 612 (7940), 477–482.
Prather, M.J., Hsu, J., Deluca, N.M., Jackman, C.H., Oman, L.D., Douglass, A.R., Fleming, E.L., Strahan, S.E., Steenrod, S.D., Søvde, O.A., Isaksen, I.S.A., Froidevaux, L., Funke, B., 2015. Measuring and modeling the lifetime of nitrous oxide including its variability. J. Geophys. Res. Atmos. 120 (5), 693–705.
Prather, M.J., Penner, J.E., Fuglestvedt, J.S., Kurosawa, A., Lowe, J.A., Höhne, N., Jain, A.K., Andronova, N., Pinguelli, L., de Campos, C.P., Raper, S.C.B., Skeie, R.B., Stott, P.A., van Aardenne, J., Wagner, F., 2009. Tracking uncertainties in the causal chain from human activities to climate. Geophys. Res. Lett. 36 (5), 1–6, 2009.
Qing, X., Qi, B., Lin, Y., Chen, Y., Zang, K., Liu, S., Ma, Q., Qiu, S., Jiang, K., Xiong, H., Li, J., Hong, H., Niu, Y., Du, R., Zhang, H., Fang, S., 2022. Characteristics of the

methane (CH_4) mole fraction in a typical city and suburban site in the Yangtze River Delta. China. Atmos. Pollut. Res. 13 (8), 101498.
Razif, M., Santoso, I.B., 2016. Prediction of CO, CO_2, CH_4, and N_2O vehicle emissions from environmental impact assessment (EIA) at toll road of Krian-Legundi-Bunder in East Java of Indonesia. Int. J. Chemtech. Res. 9 (3), 653–664.
Ren, S., Fu, X., Chen, X., 2012. Regional variation of energy-related industrial CO_2 emissions mitigation in China. China Econ. Rev. 23 (4), 1134–1145.
Rella, C.W., Chen, H., Andrews, A.E., Filges, A., Gerbig, C., Hatakka, J., Karion, A., Miles, N.L., Richardson, S.J., Steinbacher, M., Sweeney, C., Wastine, B., Zellweger, C., 2013. High accuracy measurements of dry mole fractions of carbon dioxide and methane in humid air. Atmos. Meas. Tech. 6 (3), 837–860.
Reum, F., Gerbig, C., Lavric, J.V., Rella, C.W., Göckede, M., 2019. Correcting atmospheric CO_2 and CH_4 mole fractions obtained with Picarro analyzers for sensitivity of cavity pressure to water vapor. Atmos. Meas. Tech. 12 (2), 1013–1027.
Schmidt, M., Graul, R., Sartorius, H., Levin, I., 1996. Carbon dioxide and methane in continental Europe: a climatology, and ^{222}Radon-based emission estimates. Tellus B 48 (4), 457–473. https://doi.org/10.1034/j.1600-0889.1994.t01-2-00002.x-i1.
Sha, T., Ma, X., Jia, H., van der A, R., Ding, J., Zhang, Y., Chang, Y., 2019. Exploring the influence of two inventories on simulated air pollutants during winter over the Yangtze River Delta. Atmos. Environ. 206, 170–182. https://doi.org/10.1016/j.atmosenv.2019.03.006.
Shan, Y., Guan, D., Zheng, H., Qu, J., Li, Y., Meng, J., Mi, Z., Liu, Z., Zhang, Q., 2018. China CO_2 emission accounts 1997–2015. Sci. Data 5 (1), 1–14.
Shen, S., Yang, D., Xiao, W., Liu, S., Lee, X., 2014. Constraining anthropogenic CH_4 emissions in Nanjing and the Yangtze River Delta, China, using atmospheric CO_2 and CH_4 mixing ratios. Adv. Atmos. Sci. 31 (6), 1343–1352.
Shindell, D., Borgford-Parnell, N., Brauer, M., Haines, A., Kuylenstierna, J.C.I., Leonard, S.A., Ramanathan, V., Ravishankara, A., Amann, M., Srivastava, L., 2017. A climate policy pathway for near-and long-term benefits. Science 356 (6337), 493–494.
Song, T., Wang, Y., Sun, Y., 2013. Estimation of carbon dioxide flux and source partitioning over Beijing, China. J. Environ. Sci. 25 (12), 2429–2434.
Stavert, A.R., O'doherty, S., Stanley, K., Young, D., Manning, A.J., Lunt, M.F., Rennick, C., Arnold, T., 2019. UK greenhouse gas measurements at two new tall towers for aiding emissions verification. Atmos. Meas. Tech. 12 (8), 4495–4518.
Tong, D., Zhang, Q., Zheng, Y., Caldeira, K., Shearer, C., Hong, C., Qin, Y., Davis, S.J., 2019. Committed emissions from existing energy infrastructure jeopardize 1.5 °C climate target. Nature 572 (7769), 373–377.
Trivett, N., Worthy, D.E.J., Brice, K.A., 1989. Surface measurements of carbon dioxide and methane at Alert during an arctic haze event in April, 1986. J. Atmos. Chem. 9 (1), 383–397.
Turner, A.J., Frankenberg, C., Kort, E.A., 2019. Interpreting contemporary trends in atmospheric methane. Proc. Natl. Acad. Sci. USA 116 (8), 2805–2813.
Wallington, T., Wiesen, P., 2014. N_2O emissions from global transportation. Atmos. Environ. 94, 258–263.
Wang, F., Maksyutov, S., Janardanan, R., Tsuruta, A., Ito, A., Morino, I., Yoshida, Y., Tohjima, Y., Kaiser, J.W., Lan, X., Zhang, Y., Mammarella, I., Lavric, J.V., Matsunaga, T., 2022. Atmospheric observations suggest methane emissions in north-eastern China growing with natural gas use. Sci. Rep. 12 (1), 18587.
Wang, J., Cai, B., Zhang, L., Cao, D., Liu, L., Zhou, Y., Zhang, Z., Xue, W., 2014. High-resolution carbon dioxide emission gridded data for China derived from point sources. Environ. Sci. Technol. 48 (12), 7085–7093.
Wang, Y., Broquet, G., Bréon, F.M., Lespinas, F., Buchwitz, M., Reuter, M., Meijer, Y., Loescher, A., Janssens-Maenhout, G., Zheng, B., Ciais, P., 2020. PMIF v1.0: assessing the potential of satellite observations to constrain CO_2 emissions from large cities and point sources over the globe using synthetic data. Geosci. Model Dev. (GMD) 13 (11), 5813–5831.
Wang, Y., Wang, C., Guo, X., Liu, G., Huang, Y., 2002. Trend, seasonal and diurnal variations of atmospheric CO_2 in Beijing. Chin. Sci. Bull. 47 (24), 2050–2055.
Wang, R., Tao, S., Ciais, P., Shen, H.Z., Huang, Y., Chen, H., Shen, G.F., Wang, B., Li, W., Zhang, Y.Y., Lu, Y., Zhu, D., Chen, Y.C., Liu, X.P., Wang, W.T., Wang, X.L., Liu, W.X., Li, B.G., Piao, S.L., 2013. High-resolution mapping of combustion processes and implications for CO_2 emissions. Atmos. Chem. Phys. 13 (10), 5189–5203.
Wennberg, P.O., Mui, W., Wunch, D., Kort, E.A., Blake, D.R., Atlas, E.L., Santoni, G.W., Wofsy, S.C., Diskin, G.S., Jeong, S., Fischer, M.L., 2012. On the sources of methane to the Los Angeles atmosphere. Environ. Sci. Technol. 46 (17), 9282–9289.
Wong, K.W., Fu, D., Pongetti, T.J., et al., 2015. Mapping CH_4:CO_2 ratios in Los Angeles with CLARS-FTS from Mount Wilson, California. Atmos. Chem. Phys. 15 (1), 241–252.
Worthy, D.E.J., Trivett, N.B.A., Hopper, J.F., Bottenheim, J.W., Levin, I., 1994. Analysis of long-range transport events at alert, Northwest Territories, during the Polar Sunrise experiment. J. Geophys. Res. Atmos. 99 (D12), 25329–25344.
Wunch, D., Wennberg, P.O., Toon, G.C., Keppel-Aleks, G., Yavin, Y.G., 2009. Emissions of greenhouse gases from a North American megacity. Geophys. Res. Lett. 36 (15), 1–5. https://doi.org/10.1029/2009GL039825.
Xu, J., Lee, X., Xiao, W., Cao, C., Liu, S., Wen, X., Xu, J., Zhang, Z., Zhao, J., 2017. Interpreting the $^{13}C/^{12}C$ ratio of carbon dioxide in an urban airshed in the Yangtze River Delta, China. Atmos. Chem. Phys. 17 (5), 3385–3399.
Yan, H., Xie, L., Guo, L., Fan, J., Diao, T., Lin, M., Zhang, H., Lin, E., 2014. Characteristics of nitrous oxide emissions and the affecting factors from vegetable fields on the North China Plain. J. Environ. Manag. 144, 316–321.
Yan, X., Qiu, D., Guo, D., Qi, X., Zheng, S., Cheng, K., Sun, J., Zheng, J., 2018. Emission inventory of greenhouse gas from urban wastewater treatment plants and its temporal and spatial distribution in China. Environ. Sci. 39 (3), 1256–1263 (in Chinese).
Yang, Y., Ren, L., Wu, M., Wang, H., Song, F., Leung, L.R., Hao, X., Li, J., Chen, L., Li, H., Zeng, L., Zhou, Y., Wang, P., Liao, H., Wang, J., Zhou, Z., 2022. Abrupt emissions reductions during COVID-19 contributed to record summer rainfall in China. Nat. Commun. 13 (1), 1–7, 959.
Yver-Kwok, C., Philippon, C., Bergamaschi, P., Biermann, T., Calzolari, F., Chen, H., Conil, S., Cristofanelli, P., Delmotte, M., Hatakka, J., Heliasz, M., Hermansen, O., Kominkova, K., Kubistin, D., Kumps, N., Laurent, O., Laurila, T., Lehner, I., Levula, J., Lindauer, M., Lopez, M., Mammarella, I., Manca, G., Marklund, P., Metzger, J.M., Mélder, M., Platt, S.M., Ramonet, M., Rivier, L., Scheeren, B., Shall, M.K., Smith, P., Steinbacher, M., Vitkova, G., Wyss, S., 2021. Evaluation and optimization of ICOS atmosphere station data as part of the labeling process. Atmos. Meas. Tech. 14 (1), 89–116.
Zazzeri, G., Lowry, D., Fisher, R.E., France, J.L., Lanoisellé, M., Grimmond, C.S.B., Nisbet, E.G., 2017. Evaluating methane inventories by isotopic analysis in the London region. Sci. Rep. 7 (1), 4854.
Zhang, H., Ma, X., Han, G., Xu, H., Shi, T., Zhong, W., Gong, W., 2021. Study on collaborative emission reduction in green-house and pollutant gas due to COVID-19 lockdown in China. Remote Sens. 13 (17), 1–17, 3492.
Zhang, P., Zhang, L., Tian, X., et al., 2018. Urban energy transition in China: insights from trends, socioeconomic drivers, and environmental impacts of Beijing. Energy Policy 117, 173–183.
Zheng, B., Geng, G., Ciais, P., Davis, S.J., Martin, R.V., Meng, J., Wu, N., Chevallier, F., Broquet, G., Boersma, F., van der A, R., Lin, J., Guan, D., Lei, Y., He, K., Zhang, Q., 2020. Satellite-based estimates of decline and rebound in China's CO_2 emissions during COVID-19 pandemic. Sci. Adv. 6 (49) eabd4998.
Zheng, B., Tong, D., Li, M., et al., 2018. Trends in China's anthropogenic emissions since 2010 as the consequence of clean air actions. Atmos. Chem. Phys. 18 (19), 14095–14111.
Zhao, Y., Saunois, M., Bousquet, P., Lin, X., Berchet, A., Hegglin, M.I., Canadell, J.G., Jackson, R.B., Deushi, M., Jöckel, P., Kinnison, D., Kirner, O., Strode, S., Tilmes, S., Dlugokencky, E.J., Zheng, B., 2020. On the role of trend and variability of hydroxyl radical (OH) in the global methane budget. Atmos. Chem. Phys. 20, 13011–13022.
Zhou, Y., 2020. Processes and enlightenment of urban-rural clean heating in Beijing. Environ. Sustain. Dev. 45 (3), 57–66 (in Chinese).
Zhou, X., Yang, F., Yang, F., Feng, D., Pan, T., Liao, H., 2022. Analyzing greenhouse gas emissions from municipal wastewater treatment plants using pollutants parameter normalizing method: a case study of Beijing. J. Clean. Prod. 376, 134093.